NeuroImage 145 (2017) 58–73

Contents lists available at ScienceDirect

NeuroImage

journal homepage: www.elsevier.com/locate/neuroimage

Perceived social isolation is associated with altered functional connectivity in neural networks associated with tonic alertness and executive control

Elliot A. Layden[a,b,*], John T. Cacioppo[a,b], Stephanie Cacioppo[b,c], Stefano F. Cappa[d,e], Alessandra Dodich[e], Andrea Falini[f,g], Nicola Canessa[d,e]

[a] Department of Psychology, The University of Chicago, Chicago, IL 60637, United States
[b] Center for Cognitive and Social Neuroscience, The University of Chicago, Chicago, IL 60637, United States
[c] Biological Sciences Division, The University of Chicago Pritzker School of Medicine, Chicago, IL 60637, United States
[d] NEtS Center, Scuola Universitaria Superiore IUSS, Pavia 27100, Italy
[e] Cognitive Neuroscience Unit, Division of Neuroscience, IRCCS Ospedale San Raffaele, Milan 20132, Italy
[f] Department of Neuroradiology, IRCCS Ospedale San Raffaele, Milan 20132, Italy
[g] CERMAC, Division of Neuroscience, IRCCS Ospedale San Raffaele, Milan 20132, Italy

ARTICLE INFO

Keywords:
Perceived social isolation
Resting-state fMRI
Attention
Functional connectivity
Loneliness

ABSTRACT

Perceived social isolation (PSI), colloquially known as loneliness, is associated with selectively altered attentional, cognitive, and affective processes in humans, but the neural mechanisms underlying these adjustments remain largely unexplored. Behavioral, eye tracking, and neuroimaging research has identified associations between PSI and implicit hypervigilance for social threats. Additionally, selective executive dysfunction has been evidenced by reduced prepotent response inhibition in social Stroop and dichotic listening tasks. Given that PSI is associated with pre-attentional processes, PSI may also be related to altered resting-state functional connectivity (FC) in the brain. Therefore, we conducted the first resting-state fMRI FC study of PSI in healthy young adults. Five-minute resting-state scans were obtained from 55 participants (31 females). Analyses revealed robust associations between PSI and increased brain-wide FC in areas encompassing the right central operculum and right supramarginal gyrus, and these associations were not explained by depressive symptomatology, objective isolation, or demographics. Further analyses revealed that PSI was associated with increased FC between several nodes of the cingulo-opercular network, a network known to underlie the maintenance of tonic alertness. These regions encompassed the bilateral insula/frontoparietal opercula and ACC/pre-SMA. In contrast, FC between the cingulo-opercular network and right middle/superior frontal gyrus was reduced, a finding associated with diminished executive function in prior literature. We suggest that, in PSI, increased within-network cingulo-opercular FC may be associated with hypervigilance to social threat, whereas reduced right middle/superior frontal gyrus FC to the cingulo-opercular network may be associated with diminished impulse control.

Introduction

Social isolation has been recognized as a major risk factor for morbidity and mortality in humans for more than a quarter of a century (Cacioppo et al., 2015). Efforts to explain this association have often focused on objective social roles and health behaviors. However, population-based longitudinal research indicates that *perceived* social isolation (PSI; colloquially known as loneliness) is a major risk factor for morbidity and mortality, independent of objective social isolation and health behaviors (Cacioppo et al., 2015; Cacioppo et al., 2002; Cacioppo et al., 2014;S. Cacioppo et al., 2015; Holt-Lunstad et al., 2015). Furthermore, PSI is associated with increased risk of developing dementia (Holwerda et al., 2014), and a more than two-fold increased risk of developing clinical Alzheimer's disease (Wilson et al., 2007), independent of objective social isolation. Given that the brain is the key organ for forming, monitoring, maintaining, repairing, and replacing salutary connections with others (Cacioppo et al., 2015), a growing body of multidisciplinary research seeks to understand the neural underpinnings of PSI (for review, see Cacioppo and Cacioppo, 2016; Cacioppo et al. 2014).

Human structural neuroimaging, using voxel-based morphometry (VBM) and diffusion tensor imaging (DTI), has yielded important

* Corresponding author at: The Center for Cognitive and Social Neuroscience (CCSN), 940 E. 57th Street, 4th Floor, Room 427, Chicago, IL 60637, United States.
E-mail address: elayden@uchicago.edu (E.A. Layden).

http://dx.doi.org/10.1016/j.neuroimage.2016.09.050
Received 29 March 2016; Accepted 20 September 2016
Available online 21 September 2016
1053-8119/

insights in this respect. For instance, Kanai et al. (2012) used VBM to identify an association between PSI and decreased regional grey matter volume (rGMV) in the left posterior superior temporal sulcus (pSTS), a region associated with basic social perception skills. In another VBM study, Nakagawa et al. (2015) lent further support to this finding by demonstrating an association between PSI and reduced regional white matter volume in a left pSTS cluster, in addition to reductions near the bilateral inferior parietal lobule, right anterior insula, posterior temporoparietal junction (TPJ), rostrolateral and dorsomedial prefrontal cortex. These latter findings were interpreted as relating to reduced empathy and self-efficacy in PSI (Nakagawa et al., 2015). However, the ventral attention network (VAN), comprised primarily of the TPJ and ventral frontal cortex (Corbetta and Shulman, 2002), also seems to have been implicated. Consistent with this observation, Tian et al. (2014) reported reduced fractional anisotropy among several right-lateralized white matter tracts of the VAN in a DTI investigation of PSI. Finally, Kong et al. (2015) used VBM to identify an association between PSI and increased rGMV in the left dorsolateral prefrontal cortex (DLPFC), which was thought to be associated with emotional regulation deficits and executive dysfunction.

Functional neuroimaging has also recently yielded several important insights for our understanding of PSI. For instance, a study of older adults found that late-life depression significantly moderated associations between PSI and task-based fMRI functional connectivity (FC) in a distributed network of regions during an emotional processing task (Wong et al., 2016). Additionally, in a sample of older males, Lan et al. (2015) found evidence for an association between PSI and increased short-range functional connectivity density (Tomasi and Volkow, 2010) in a bilateral lingual gyrus cluster, a region associated with social cognition. However, the generalizability of these findings to other demographic groups is uncertain given the specific sampling characteristics.

In the first neuroimaging study of PSI, Cacioppo et al. (2009) found that PSI was associated with increased bilateral visual cortex fMRI activity in response to viewing unpleasant social, compared to unpleasant non-social, pictures. This finding has been interpreted as evidence of an implicit hypervigilance to social threats in PSI, a pre-attentive bias which has been consistently identified using a variety of methods (Bangee et al., 2014; Cacioppo et al., 2009, 2014; Cacioppo and Hawkley, 2009; Cacioppo and Patrick, 2008; Cacioppo et al., 2014; Qualter et al., 2013). Subsequent electrical neuroimaging studies have found that individuals high in PSI more quickly process and differentiate threatening social from threatening non-social images (Cacioppo et al., 2015). This was also confirmed in a separate paradigm which compared negative social to negative non-social words in a modified social Stroop task (Cacioppo et al., 2015). These differences in the early processing of threatening social information, which are thought to be largely implicit and non-conscious, would seem to suggest altered resting-state brain networks which prepare high PSI individuals for faster detection of social threats.

Resting-state fMRI FC analyses have proven invaluable research tools for investigating neural phenomena underlying stably altered attention, cognition, and behavior in humans (Van Den Heuvel and Pol, 2010). Thus, we implemented this methodology to investigate the extent to which resting-state neural networks are associated with tonic PSI. Specifically, we sought to investigate the extent to which the implicit hypervigilance for social threats that characterizes PSI is reflected in the FC of the resting brain. Based on the existing neuroimaging and behavioral research, we posited that PSI would be associated with altered resting-state FC within brain networks underlying attention, such as the VAN, the dorsal attention network, or the cingulo-opercular network (for review, see Petersen and Posner, 2012). To improve the specificity of any observed associations, and to investigate putative mediational effects, we also measured depressive symptomatology, objective social isolation, and demographic variables. Furthermore, we undertook ancillary analyses to statistically test for hemispheric lateralization of any FC associations observed. Notably, this study represents the first investigation of altered resting-state FC associated with PSI in a sample of healthy young adults, to the best of our knowledge.

Methods

Participants

Fifty-five right-handed (Oldfield, 1971) healthy volunteers (24 males; 31 females; mean age=23.7; SD=2.1) participated in the study. All subjects had normal or corrected visual acuity. None reported a history of neuropsychiatric conditions or substance abuse, nor were any currently taking any medication which interferes with cognitive functioning. All participants gave written informed consent to the experimental procedure, which was approved by the local Ethics Committee.

Assessment of behavioral measures

Perceived social isolation

PSI was assessed using the revised UCLA Loneliness Scale (R-UCLA), a widely used and reliable self-report measure (Russell, 1996). The scale consists of 20 items probing satisfaction with social relationships. An example item is, “How often do you feel that there is no one you can turn to?” Each item is rated on a 4-point Likert-type scale, where 1=Never, 2=Rarely, 3=Sometimes, and 4=Often. Total PSI scores are calculated by summing items, reverse coding where necessary so that higher scores correspond to higher PSI. Total scores can range from 20 to 80. The R-UCLA scale demonstrated high internal consistency in our sample (Cronbach's α=.89). PSI was treated as a continuous variable in this study, and any references to high or low PSI are made relative only to our specific sampling distribution. The mean and standard deviation of PSI scores can be found in Table 1.

Additional covariates

To assure the specificity of findings to our criterion variable, PSI, and to test for possible mediation effects, four additional covariates were assessed. These consisted of self-reported age and gender, as well as two additional behavioral measures, objective social isolation and depressive symptomatology. All covariates, with the exception of gender, were treated as continuous variables.

Objective social isolation

A measure of objective social isolation consists of how much contact respondents have with others, irrespective of their subjective feelings, including PSI, which may accompany level of contact. To assess isolation, we used the scale implemented by Steptoe et al. (2013). In their study, isolation showed a small, positive correlation with PSI (r=0.10, $p < 0.001$). The Steptoe et al. (2013) measure asks respondents if they are unmarried/not cohabiting; have less than monthly contact with each of children, other family members, and friends; and if they participate in organizations such as social clubs, religious

Table 1
Sample demographics.

Demographic variable	Mean ± SD	Range
Age	23.7 ± 2.1	20–29
Gender	*n*	%
Male	24	43.6
Female	31	56.4
Psychometric variable	Mean	SD
PSI (R-UCLA)	40	8.1
CES-D-ML	16.2	10.4
Objective isolation	1.4	0.7

groups, or committees. To calculate a respondent's total score, one point is added for each form of isolation selected by the respondent. Total scores can range from 0-5. The mean and standard deviation of isolation scores can be found in Table 1.

Depressive symptomatology

We assessed depressive symptomatology using the CES-D scale (Radloff, 1977). The CES-D contains one item which directly addresses PSI ("I felt lonely"). This item was dropped because factor analyses have shown it to inflate the association between PSI and depressive symptomatology (Cacioppo et al., 2006). This edited version of the scale has been referred to in the literature as the CES-D-ML (CES-D minus loneliness) scale (Cacioppo et al., 2006). The CES-D-ML scale instructs participants to indicate how frequently they have experienced various components of depressive symptomatology during the past week. An example item is, "I felt that everything I did was an effort." Each item is rated using response options of 0 ("Rarely or None of the Time (Less than 1 Day)"), 1 ("Some or a Little of the Time (1–2 Days)"), 2 ("Occasionally or a Moderate Amount of Time (3–4 Days)"), and 3 ("Most or All of the Time (5–7 Days)"). An individual's total score is calculated by summing across items, reverse coding where necessary so that higher scores corresponded to greater depressive symptomatology. Total scores for the CES-D-ML can range from 0-57. The scale demonstrated high internal consistency in our sample (Cronbach's α=.91). The mean and standard deviation of depressive symptomatology scores can be found in Table 1.

Imaging data acquisition and preprocessing

R-fMRI data collection

Neuroimaging was conducted at IRCCS Ospedale San Raffaele in Milan, Italy. Functional T2*-weighted MR images were collected using a 3 Tesla Philips Achieva scanner (Philips Medical Systems, Best, NL), using an 8-channel SENSE head coil (sense reduction factor=2). Functional images were acquired using a T2*-weighted gradient-echo, echo-planar pulse sequence (37 continuous ascending transverse slices covering the whole brain, tilted 30° downward with respect to the bicommissural line to reduce susceptibility artifacts in orbitofrontal regions; TR=2000 ms, TE=30 ms, flip-angle=85°, FOV=192 mm× 192 mm, slice thickness=3.7 mm, interslice gap=0.55 mm, in-plane resolution=2 mm×2 mm). Resting-state scans included 150 volumes, corresponding to 5 minutes. The beginning of this scan was preceded by the collection of 6 "dummy" functional volumes, covering the amount of time needed to allow for T1-equilibration effects, which were automatically discarded. Participants were instructed to lie quietly with their eyes open and stare passively at a foveally presented grey fixation cross. This procedure has been shown to facilitate network delineation compared to eyes-closed conditions (Van Dijk et al., 2010).

R-fMRI data preprocessing

Image pre-processing was performed using SPM8 (http://www.fil.ion.ucl.ac.uk/spm), implemented in Matlab v7.4 (Mathworks, Inc., Sherborn, MA) (Worsley and Friston, 1995). The 150 volumes from each subject underwent a standard spatial pre-processing including spatial realignment to the first volume and unwarping, slice-timing correction with the middle slice in time as a reference, spatial normalization into the standard Montreal Neurological Institute (MNI) space (Friston et al., 1995), resampling to 2×2×2 mm^3 voxels, as well as spatial smoothing using a 8 mm full-width half-maximum (FWHM) isotropic Gaussian kernel. We assessed the quality and consistency of spatial normalization by computing the Spearman correlation between the SPM EPI template and the mean image of the smoothed, normalized functional volumes. For all subjects the resulting correlation index was above 0.95 (mean=0.969; standard deviation=0.002), indicating a robust and consistent spatial normalization. We used the Motion Fingerprint toolbox (Wilke, 2012, 2014; http://www.medizin.uni-tuebingen.de/kinder/en/research/neuroimaging/software/) to compute, for each subject, a comprehensive indicator of scan-to-scan head motion which was subsequently modeled as a nuisance predictor in statistical analyses.

Brain mask creation

A brain mask in which to confine analyses was created by first segmenting the normalized anatomical volume of each subject into tissue probability maps for grey matter (GM), white matter (WM), and cerebrospinal fluid (CSF) using SPM8. GM probability maps were averaged across subjects and thresholded at a cutoff of at least .2 probability (e.g., Dai et al., 2014). Due to inherent imperfections in spatial normalization procedures, binary masks obtained via averaging across subjects tend to exclude some voxels which contain GM in a subset of subjects; additionally, as a consequence of spatial smoothing, voxels at the GM-WM interface likely contain substantial spillover GM signals (Thyreau et al., 2012). Thus, to ensure that GM regions and signals are not erroneously excluded from the brain mask, which can increase false-negatives in neuroimaging studies (Ridgway et al., 2009), the interior of the .2 binary GM mask was volume-filled using custom Matlab scripts (version R2014a, Mathworks, Inc., Sherborn, MA). Then, voxels where at least 90% of subjects demonstrated a .5 probability or greater of containing either WM or CSF were masked out from this volume. This resulted in a brain mask containing 187,410 voxels.[1]

Denoising of voxel-wise time series

Voxel-wise time series were further processed using denoising steps implemented by CONN Toolbox, version 15c (Whitfield-Gabrieli and Nieto-Castanon, 2012). These statistically remove several nuisance covariates from time series (ramp-up effects in the magnetic resonance signal, linear drift, subject-specific head motion parameters, and physiological noise related to cardiac, respiratory, and other sources). Specifically, the aCompCorr method (Behzadi et al., 2007; Whitfield-Gabrieli and Nieto-Castanon, 2012) was used to remove physiological noise without regressing out the global grey matter signal. This is advantageous because global signal regression is thought to introduce a large number of possibly spurious negative correlations when computing FC (Murphy et al., 2009; Weissenbacher et al., 2009). The aCompCorr approach defines noise regions of interest (ROIs) as stringently thresholded WM and CSF masks, with WM further eroded by two voxels in each direction to avoid including partial volume regions. The first sixteen principal components (the default number in CONN Toolbox, ver. 15c) were extracted for each subject from the voxel-wise time series of the WM and CSF noise ROIs. These components, along with subject-specific motion parameters, a linear detrending term, and a term accounting for ramp-up effects in the magnetic resonance signal, were included as nuisance regressors in a general linear model (GLM), with each in-mask voxel time series

[1] Greater inclusiveness of GM voxels in the analysis mask may also mean including more WM and GM-WM interface voxels. Partial volume effects can confound FC analyses if these latter tissues have reduced correlations with other brain voxels due to increased noise variability (Dukart and Bertolino, 2014). This source of variation was not expected to play a major role in determining FC in the current study, because our sample consisted of healthy young adults, rather than a clinical population where grey matter atrophy could confound comparisons with a control group (Dukart and Bertolino, 2014). However, we conducted an analysis to ensure that our results were not affected by variation in brain tissue distribution across participants: within-subjects regression analyses were implemented to statistically control ICC maps for underlying brain tissue distribution. For each subject, a multiple regression model was specified with ICC across in-mask voxels as the criterion variable, and GM, WM, and CSF probability at corresponding voxels as predictors. The maximum percentage of ICC variance explained by these models for any subject was 4.11%. The average variance explained across-subjects was 1.56%. We retained the residuals from these regressions for each subject, repeating our main ICC analyses using these residuals in place of the original ICC scores. This change did not qualitatively affect the significant clusters obtained. For more information, please contact the corresponding author.

specified as the criterion variable. The residual time series obtained from regression were then band-pass filtered (range: .008 to .09 Hz). We performed band-pass filtering after nuisance regression due to the observation that performing these steps in the opposite order reintroduces nuisance-related variation into the time series and overestimates brain-wide FC (Hallquist et al., 2013).

Imaging data analysis

Intrinsic connectivity contrast (ICC) analysis

A data-driven approach was used to investigate associations between regional brain-wide FC strength and PSI. The Intrinsic Connectivity Contrast (ICC) is a metric similar to connectivity strength from graph theory (Martuzzi et al., 2011; Rubinov and Sporns, 2010). This class of measures has proven useful for identifying brain regions which are maximally functionally connected to the rest of the brain, and which may be integral to the coordination of large-scale patterns of brain activity (Buckner et al., 2009; Cole et al., 2010; Anticevic et al., 2014). ICC differs from strength, however, by requiring no thresholding of correlations, and thus no a priori knowledge or assumptions (Martuzzi et al., 2011). ICC is computed at each voxel by averaging the squared, Fisher's z-transformed, Pearson correlation between a given voxel time series and that of every other in-mask voxel (Martuzzi et al., 2011). A positive association between PSI and ICC may suggest that a region is overly connected with broad areas of the brain in subjects experiencing PSI, whereas a negative association may imply that a region has decreased participation in large-scale brain networks for subjects experiencing PSI (Anticevic et al., 2014). Similar measures have recently been used to investigate regional FC associations in Alzheimer's disease (Dai et al., 2014; Buckner et al., 2009), major depressive disorder (Marchand et al., 2013; Wang et al., 2014), and obsessive compulsive disorder (Anticevic et al., 2014).

Here, we implemented ICC analyses using CONN Toolbox. Whole-brain ICC maps were computed for each subject, wherein the intensity at each voxel quantified its overall level of functional connectedness to the rest of the brain. ICC maps were converted to standard scores within-subjects and submitted to GLM analyses. First, to assess the bivariate relationship between ICC and PSI, ICC maps across subjects were modeled as the criterion variable, and PSI was modeled as the predictor. Second, the relationship between ICC and PSI was reassessed holding age, gender, isolation, and CES-D-ML scores constant. In each case, a two-tailed contrast was computed at every voxel for the regression coefficient estimate obtained for PSI. Clusters of voxels where intrinsic FC was significantly associated with PSI were identified using the Monte Carlo simulation-based nonstationary supra-threshold cluster-size approach (Hayasaka et al., 2004). A primary threshold of p-uncorrected $< .005$ was adopted (Woo et al., 2014), and results were corrected for multiple comparisons using a family-wise error (FWE) corrected extent threshold of $p < .05$. For the former contrast, this meant that voxels needed to surpass a threshold of $t(1,53) \geq 2.93$ or ≤ 2.93 to be incorporated into clusters, and clusters were required to contain at least $k=197$ suprathreshold, spatially-contiguous voxels to be deemed significant. The corresponding thresholds for the latter contrast were $t(1,49) \geq 2.94$ or ≤ -2.94 and $k=243$.

Prediction of PSI using ICC

A regression analysis was undertaken to estimate the efficacy of ICC for predicting PSI. For each subject, the average ICC score was extracted across the component voxels of each cluster identified in the bivariate contrast above. These average ICC scores were used in between-subjects regressions predicting PSI. First, each cluster was separately modeled as a predictor in a simple regression, with PSI as the criterion variable. Second, a multiple regression model was specified to examine the prediction efficacy of cluster ICC, holding constant demographic and behavioral variables. Finally, to examine whether each cluster contributed unique information to predictions of PSI, a multiple regression model was specified, entering both ICC clusters simultaneously as predictors and PSI as the criterion variable. This was repeated a second time, additionally entering demographic and behavioral variables as covariates.

Mediation analyses

To determine whether any behavioral or demographic covariates mediated the ability for PSI scores to predict ICC scores averaged over clusters identified by ICC analyses, we conducted a series of mediation analyses using the Mediation Toolbox (Wager, 2006: http://wagerlab.colorado.edu/wiki/doku.php/help/mediation/m3_mediation_fmri_toolbox).

For each covariate and each cluster, we constructed a distribution of path coefficients, including the indirect effect, using 10,000 bootstrap samples. These distributions allowed us to non-parametrically test whether a given covariate mediated the association between PSI and ICC at a given cluster.

Mediation analysis for depressive symptomatology

Due to prior literature showing that PSI significantly predicts later depressive symptomatology in cross-lagged analyses (Cacioppo et al., 2010), we conducted further mediation analyses specifically involving this covariate. Namely, we tested whether depressive symptomatology predicted average ICC at the clusters identified, and if this association was mediated by PSI scores. Also, reversing the direction of inference, we tested whether average ICC at a given cluster predicted PSI or depressive symptomatology, and secondly, whether the other respective covariate mediated the association.

Cluster-wise mediation

We conducted an additional mediation analysis to investigate whether the ability of average ICC of a given cluster to predict PSI scores was mediated by the average ICC of any other cluster identified by ICC analyses. If the association between ICC at one cluster and PSI was mediated by the ICC of a different cluster, this may lend convergent evidence, along with other analyses described below, supporting the notion that two clusters are related to PSI via a broader network in which both are embedded.

Construction of ROI-to-voxel networks

The two clusters identified in ICC analyses appeared to be located within or near regions previously implicated as parts of the cingulo-opercular network (Power et al., 2011). A key node of this network, the right anterior insula/right frontal operculum (R aI/fO; Dosenbach et al., 2006), was located directly adjacent to the right central operculum cluster identified by our ICC analyses. Thus, to further investigate the association between our results and this network, we sought to compare, both qualitatively and quantitatively, the FC maps associated with the clusters identified in our study to the FC map of the R aI/fO ROI. First, we created a 6 mm spherical ROI centered on the peak voxel coordinates reported for the R aI/fO in a previous study ([+40, +16, +4]; Dosenbach et al., 2006). Next, we extracted the average time series of this ROI for each subject and computed a Fisher's z-transformed Pearson correlation between this time series and that of every other in-mask brain voxel, creating a subject-specific brain-wide FC map. Next, we averaged these FC maps across subjects, yielding a sample-average FC map. We repeated this process for both clusters identified in bivariate ICC analyses. To facilitate qualitative comparisons, we used the cluster-extent method to threshold sample-average FC maps for each ROI, retaining only ROI-to-voxel correlations significant beyond a p-uncorrected $< 10^{-8}$ height threshold, and retaining clusters significant at a p-FWE $< 5 \cdot 10^{-7}$ cluster-extent threshold. Use of these stringent thresholds assured that the retained clusters were strongly connected to the ROIs, eliminating noise and allowing the major connectivity patterns of each ROI to be compared with one another via visual inspection. Finally, to quantitatively

compare the FC maps of different ROIs, we correlated the unthresholded sample-average FC maps between each ROI pair across all 187,410 in-mask brain voxels, yielding a simple metric of similarity between FC maps.

ROI-to-ROI connectivity analysis

Our ICC analyses evaluated associations between average whole-brain FC and PSI. However, this type of analysis is unable to enumerate which specific, regional functional associations underlie any whole-brain FC associations observed (i.e., if a cluster was found to have an association between increased brain-wide FC and the criterion variable, it is not possible to know from ICC analyses alone which specific regions have increased connectivity to the cluster). Thus, we performed an additional analysis to delineate which specific regions have altered FC to the clusters identified by ICC analyses. Clusters identified using ICC (a whole-brain connectivity measure) are expected to show broad patterns of increased or decreased FC, which are most likely to arise from FC differences within the major network in which the cluster is embedded (Anticevic et al., 2014). For this reason, we used the thresholded sample-average FC maps created for qualitative comparisons, which are maps of the most significant network connections, to create a network of ROIs. We hypothesized that ROI-to-ROI connection differences within this network would also be associated with PSI. This approach has two major advantages over a whole-brain "seed-to-voxel" analysis (e.g., Dai et al., 2014; Evans et al., 2015; Shimony et al. 2009; Whitfield-Gabrieli and Nieto-Castanon, 2012), which involves cluster-inference directly on all in-mask brain voxels: 1. it allows for a focused, network-based analysis, targeting the major networks associated with an ROI (thereby greatly reducing the multiple comparisons problem), and 2. it is less vulnerable to the pitfalls involved in inference made based upon cluster extents, such as biases toward either small or large clusters depending upon threshold choice (Woo et al., 2014).

Due to the remarkable similarity between FC maps for the right supramarginal gyrus and right central operculum clusters (see *Results*

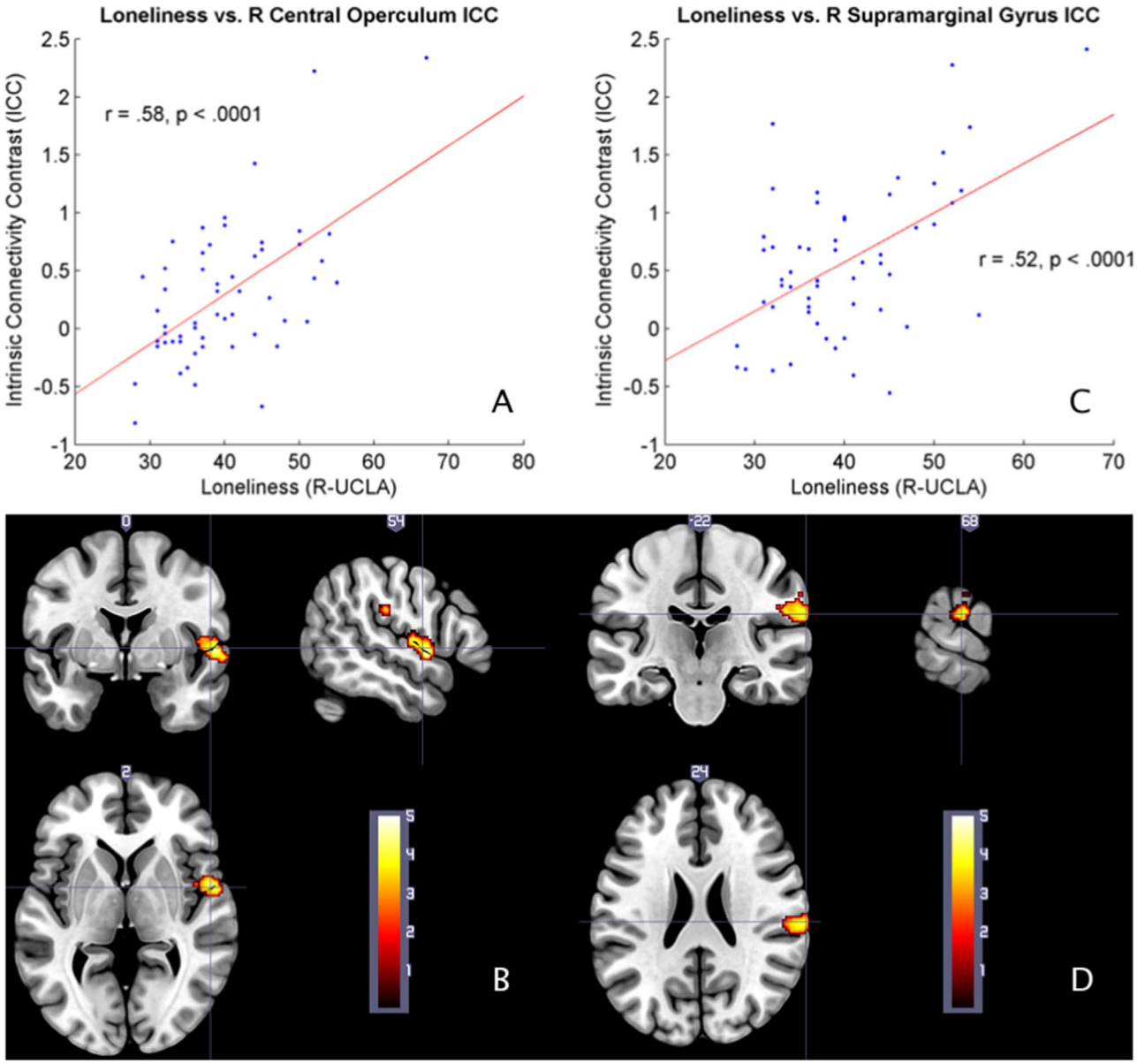

Fig. 1. Scatter plots and multi-planar slice display of two significant clusters derived from the bivariate association of ICC and loneliness. Scatter plots show average ICC values of the right central operculum cluster (**A**) and right supramarginal gyrus cluster (**C**) plotted against R-UCLA loneliness scores. Simple least-squares lines highlight the linear trend. Slice display color bars represent *t*-statistics from a two-sided contrast for the effect of loneliness on voxel-wise ICC. **B**, cluster centered on the right central opercular cortex (228 voxels; MNI peak: [+54, +2, +0]; *p*-FWE=.008). **D**, cluster centered on the right supramarginal gyrus (197 voxels; MNI peak: [+68, −22, +24]; *p*-FWE = .017). Visualization of multi-planar slice displays was performed using MRIcroGL (http://www.cabiatl.com/mricrogl/).

– *Relating results to previously identified networks*), we combined these FC maps by averaging across all in-mask voxels prior to applying the cluster-extent method to yield only the most significant clusters (height threshold: p-uncorrected $< 10^{-8}$, cluster-extent threshold: p-FWE $< 5 \cdot 10^{-7}$). This condensed network correlated across in-mask voxels with the sample-average FC map of the right central operculum

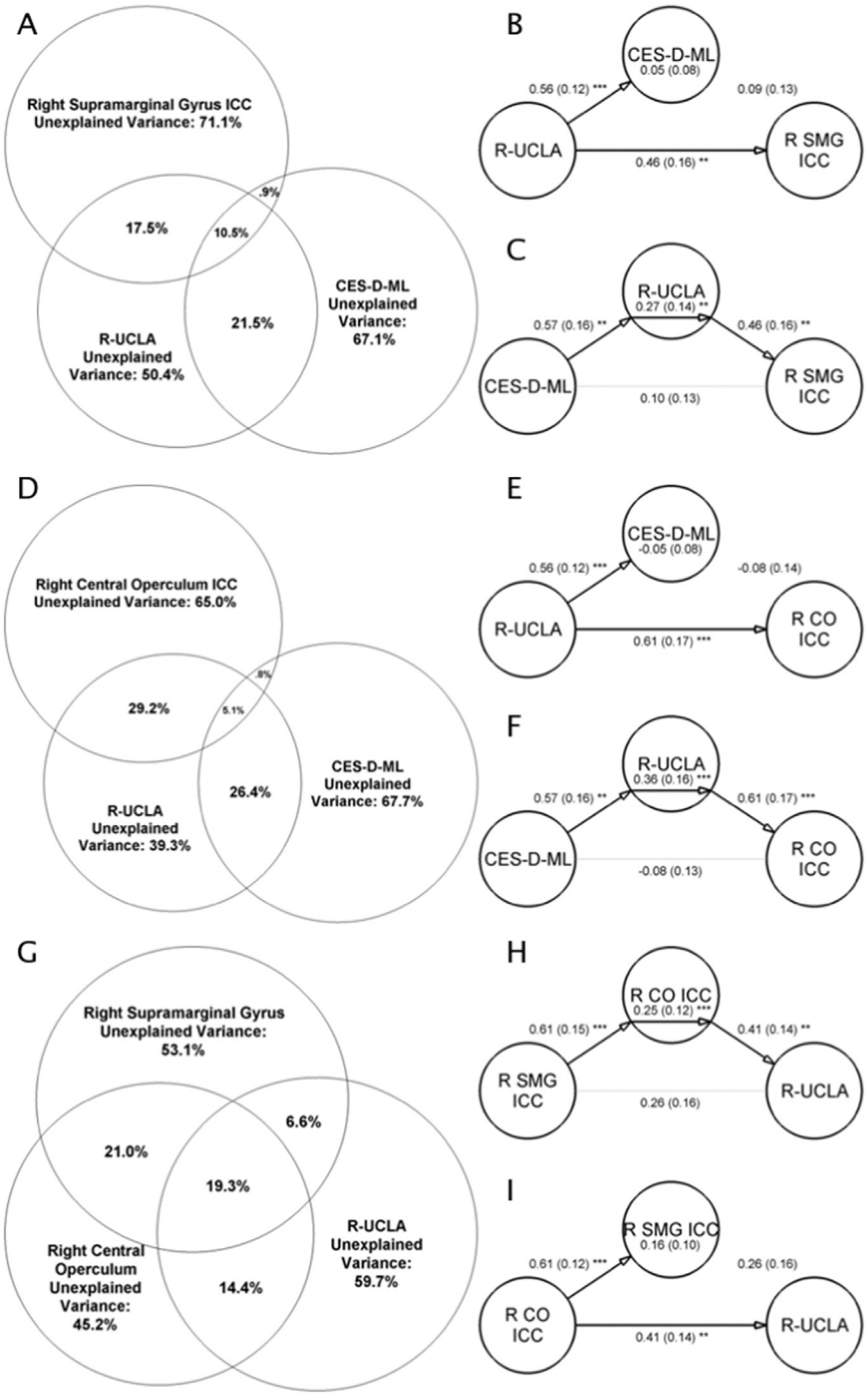

Fig. 2. Left panels (**A**, **D**, **G**) are Venn diagrams ("Ballantine diagram") which pictorially represent the unexplained variance of each variable (outer areas of each circle), the shared variance between each pair of variables, and the variance shared by all three variables (central overlap area) (Cohen et al., 2013). Total areas of each individual circle sum to one, representing the total variance of a given variable. Venn diagrams were plotted using the user-created Matlab function 'venn.m' (Gamble, 2008). Note that individual areas of the Venn diagrams may not correspond exactly to the calculated R^2 values listed; this is due to the plotting method used which attempts to maximize the visual representativeness of the diagram while allowing the exact areas to deviate slightly from input values (Chow and Rodgers, 2005). **A**, Venn diagram for visualizing the interrelations between the average intrinsic connectivity contrast scores (ICC) of the right supramarginal gyrus (R SMG), R-UCLA loneliness scores (R-UCLA), and depressive symptomatology scores (CES-D-ML). **B**, path diagrams for a mediation analysis examining whether CES-D-ML scores mediate the ability of R-UCLA scores to predict R SMG ICC. **C**, path diagrams for a mediation analysis examining whether R-UCLA scores mediate the ability of CES-D-ML scores to predict R SMG ICC. **D**, Venn diagram for visualizing the interrelations between average ICC at the right central operculum (R CO), R-UCLA scores, and CES-D-ML scores. **E**, path diagrams for a mediation analysis examining whether CES-D-ML scores mediate the ability of R-UCLA scores to predict R CO ICC. **F**, path diagrams for a mediation analysis examining whether R-UCLA scores mediate the ability of CES-D-ML scores to predict R CO ICC. **G**, Venn diagram for visualizing the interrelations between average ICC at the R SMG, average ICC at the R CO, and R-UCLA scores. **H**, path diagrams for a mediation analysis examining whether R CO ICC mediates the ability of R SMG ICC to predict R-UCLA scores. **I**, path diagrams for a mediation analysis examining whether R SMG ICC mediates the ability of R CO ICC to predict R-UCLA scores. [*, **, and *** correspond to p-values of .05, .01, and .001, respectively].

cluster at $r(187,408)=.95$, $p < 10^{-9}$, with the right supramarginal gyrus cluster FC map at $r(187,408)=.95$, $p < 10^{-9,}$ and with the R aI/fO at $r(187,408)=.57$, $p < 10^{-9}$.

The resulting clusters became our ROIs for an ROI-to-ROI network, to which we also added the ICC analysis clusters. Average signals were extracted overall voxels of each ROI, for each subject. Fisher's z-tranformed correlations were computed between each pair of average signals within-subjects. Within-subjects correlations between ROI pairs were then used as predictors for between-subjects simple regressions, with PSI modelled as the criterion variable. Regression results were corrected for multiple comparisons at a seed-level threshold of p-FDR $< .1$. To investigate whether the major nodes of the cingulo-opercular network (bilateral aI/fO and dorsal anterior cingulate cortex/medial superior frontal cortex (dACC/msFC; Dosenbach et al., 2006)) were also differentially connected with components of this network, we added these to the network and repeated analyses as before.

Results

Descriptive data analysis

Age, gender, PSI scores, CES-D-ML scores, and isolation scores for this sample are displayed in Table 1. PSI was positively correlated with depressive symptomatology ($r(53)=0.56$, $p=0.001$) but non-significantly correlated with isolation ($r(53)=.19$, $p > .15$). Depressive symptomatology demonstrated a marginal negative association with age ($r(53)=-.25$, $p=.06$). No other significant correlations were noted between covariates.

Intrinsic functional connectivity and PSI

We first performed a brain-wide analysis to investigate the association between voxel-wise intrinsic FC and PSI. A contrast for the bivariate association between PSI and ICC revealed two significant clusters of voxels where ICC was positively associated with PSI: the first encompassed parts of right central operculum and right planum polare (p-FWE=.008; cluster size=228 voxels; Peak MNI Coordinates: +54, +2, +0) (Fig. 1A, B); the second cluster primarily encompassed parts of right supramarginal gyrus, right postcentral gyrus, and right parietal operculum (p-FWE=.017; cluster size=197 voxels; Peak MNI Coordinates: +68, −22, +24) (Fig. 1C, D). The second comparison, holding covariates constant, revealed a single significant cluster which largely overlapped the right central operculum cluster from the bivariate comparison (197/243 overlapping voxels) (p-FWE=.005; cluster size=243 voxels; Peak MNI: +52, +2, +2). The right supramarginal gyrus cluster was not identified by this latter contrast.

Predicting PSI with ICC

The ICC analyses identified clusters of voxels where PSI was predictive of ICC (Fig. 1). However, from the results of these initial analyses alone, it is difficult to gauge whether our FC measure, ICC, shows efficacy for predicting PSI, or if PSI merely predicts ICC. Thus, we undertook a series of regression analyses to address this additional question. The average ICC of the right central operculum cluster significantly predicted PSI across subjects in a simple regression ($\beta=.58$, $t(53)=5.18$, $p < .001$), with the model explaining nearly 32% of variance in PSI (adjusted $R^2=.32$, $F(1, 53)=26.84$, $p < .001$). Additionally, this association remained highly significant when age, gender, CES-D-ML scores, and isolation were held constant ($\beta=.49$, $t(49)=5.09$, $p < .001$). This full model explained approximately 54% of PSI variance (adjusted $R^2=.54$, $F(1, 49)=13.54$, $p < .001$).

The average ICC of the right supramarginal gyrus cluster across subjects also significantly predicted PSI in a simple regression ($\beta=.52$, $t(53)=4.49$, $p < .001$), explaining around 26% of the variance of PSI (adjusted $R^2=.26$, $F(1, 53)=20.14$, $p < .001$). Average ICC in this cluster still significantly predicted PSI when demographic and behavioral variables were held constant ($\beta=.35$, $t(49)=3.02$, $p < .005$), with the full model explaining 41% of PSI variance (adjusted $R^2=.40$, $F(1, 49)=8.32$, $p < .001$).

To test whether each cluster contributed uniquely to PSI predictions, we entered both simultaneously as predictors in a multiple regression model predicting PSI. In this model, the right central operculum cluster ($\beta=.41$, $t(52)=2.96$, $p < .005$) was a significant predictor, but the right supramarginal gyrus cluster ($\beta=.27$, $t(52)=1.92$, $p=.06$) was only marginally significant. The full model explained approximately 36% of PSI variance (adjusted $R^2=.36$, $F(1, 52)=15.94$, $p < .001$). When demographic and behavioral covariates were entered simultaneously with the two clusters, the right supramarginal gyrus cluster became a non-significant effect ($\beta=.15$, $t(48)=1.10$, $p > .25$), whereas the right central operculum cluster remained highly significant ($\beta=.45$, $t(48)=3.24$, $p < .005$). This full model explained approximately 52% of variance in PSI scores (*adjusted* $R^2=.52$, $F(1, 48)=5.26$, $p < .001$).

Mediation analyses

No significant mediation effects were observed for any covariate (age, gender, depressive symptomatology, isolation) in terms of mediating the ability of PSI to predict the average ICC scores of the right supramarginal gyrus cluster or right central operculum cluster. Notably, neither the average ICC of the right central operculum cluster ($r(53)=-.11$, $p > .4$) or the right supramarginal gyrus cluster ($r(53)=.18$, $p > .18$) correlated significantly with objective social isolation scores. However, we conducted further tests for a conjunction of effects between PSI and objective social isolation at the request of a reviewer (see Supplementary materials, p. 4–6). The average ICC of the right central operculum and right supramarginal gyrus clusters did, on the other hand, correlate significantly with depressive symptomatology ($r(53)=.28$, $p=.04$, and $r(53)=.33$, $p=.02$, respectively). Given these latter associations, more in-depth mediational analyses were conducted specifically for depressive symptomatology, and these identified some significant partial and complete mediation effects. All coefficients reported below are standardized.

Depressive symptomatology and right supramarginal gyrus ICC

Bivariate regressions confirmed that both PSI scores ($\beta=.52$, $t(53)=4.49$, $p < .001$) and CES-D-ML scores ($\beta=.36$, $t(53)=2.80$, $p < .01$) significantly predicted average ICC at the right supramarginal gyrus across-subjects (see Fig. 2A for a Venn diagram displaying the shared variance between each variable). PSI scores still significantly predicted right supramarginal gyrus ICC when holding CES-D-ML scores constant ($\beta=.47$, $t(52)=3.33$, $p < .005$), and depressive symptomatology did not mediate this association (*indirect effect* $=.05$, $SE=.08$, $p > .3$) (Fig. 2B). However, CES-D-ML scores did not predict right supramarginal gyrus ICC when holding PSI scores constant ($\beta=.10$, $t(52)=.69$, $p > .45$), and mediation analyses revealed that PSI completely mediated this association (*indirect effect*$=.27$, $SE=.14$, $p < .01$) (Fig. 2C).

Reversing the direction of inference, we found that right supramarginal gyrus ICC significantly predicted both PSI scores ($\beta=.52$, $t(53)=4.49$, $p < .001$) and CES-D-ML scores ($\beta=.56$, $t(53)=4.89$, $p < .001$) across-subjects in bivariate regressions. Similar to previously, we found that right supramarginal gyrus ICC did not predict CES-D-ML scores when holding PSI scores constant ($\beta=.09$, $t(52)=.69$, $p > .45$), and mediation analyses revealed that PSI completely mediated this association (*indirect effect*$=.27$, $SE=.11$, $p < .005$). However, we found that, although right supramarginal gyrus ICC still significantly predicted PSI scores when holding CES-D-ML scores constant ($\beta=.37$, $t(52)=3.33$, $p < .005$), this association was partially mediated by CES-D-ML scores (*indirect effect*$=.15$, $SE=.07$, $p < .05$).

Depressive symptomatology and right central operculum ICC

For thoroughness, we repeated mediation analyses for the right central operculum cluster (See Fig. 2D for a Venn diagram displaying

the shared variance between each of this set of variables). Bivariate regressions confirmed that PSI scores (β=.58, $t(53)$=5.18, $p < .001$) significantly predicted average ICC at the right central operculum across-subjects. CES-D-ML scores only marginally predicted PSI scores (β=.26, $t(53)$=1.99, p=.052). PSI scores still significantly predicted right central operculum ICC when holding CES-D-ML scores constant (β=.63, $t(52)$=4.63, $p < .001$), and depressive symptomatology did not mediate this association (*indirect effect*=−.05, *SE*=.08, $p > .5$) (Fig. 2E). However, CES-D-ML scores did not predict right central operculum ICC when holding PSI scores constant (β=−.09, $t(52)$=−.63, $p > .5$), and mediation analyses revealed that PSI completely mediated the previously observed marginal association (*indirect effect*=.36, *SE*=.16, $p < .001$) (Fig. 2F).

Reversing the direction of inference, we found that right central operculum ICC significantly predicted PSI scores (β=.58, $t(53)$=5.18, $p < .001$) and marginally predicted CES-D-ML scores (β=.26, $t(53)$=1.99, p=.052) across-subjects in bivariate regressions. Similar to previously, we found that right central operculum ICC did not predict CES-D-ML scores when holding PSI scores constant (β=−.09, $t(52)$=−.63, $p > .5$), and mediation analyses revealed that PSI completely mediated this association (*indirect effect*=.35, *SE*=.12, $p < .001$). Right central operculum ICC still significantly predicted PSI scores when holding CES-D-ML scores constant (β=.47, $t(52)$=4.63, $p < .001$), and this association was partially mediated (marginally) by CES-D-ML scores (*indirect effect*=.12, *SE*=.07, p=.09).

Cluster-wise mediation

Results revealed that the ICC scores of the right central operculum significantly predicted ICC at the right supramarginal gyrus (β=.62, $t(53)$=5.79, $p < .001$) (See Fig. 2G for a Venn diagram displaying the shared variance between ICC at each cluster and PSI scores). Additionally, right central operculum ICC completely mediated the association between right supramarginal gyrus ICC and PSI (*indirect effect*=.25, *SE*=.12, $p < .001$) (Fig. 2H). On the other hand, right supramarginal gyrus ICC only marginally partially mediated the association between the right central operculum ICC and PSI (*indirect effect*=.16, *SE*=.10, p=.08) (Fig. 2I).

Relating results to previously identified networks

Due to a strong resemblance between our results and the cingulo-opercular network (Power et al., 2011; Dosenbach et al., 2006), we sought to thoroughly assess this resemblance both qualitatively and quantitatively. Sample-averaged FC maps for each ROI (right central operculum, right supramarginal gyrus, and R aI/fO) are displayed in Fig. 3, and the anatomical overlap of clusters contained within FC maps is displayed in Table 2A–C. The clusters displayed are limited to those which demonstrated major FC with each ROI (height threshold: p-uncorrected $< 10^{-8}$ cluster-extent threshold: p-FWE $< 5 \cdot 10^{-7}$). Visual inspection revealed marked similarity among FC maps, with commonalities including major positive FC between our seed regions and bilateral insula and operculum, positive FC with the anterior cingulate cortex (ACC) and nearby medial pre-supplementary motor area (pre-SMA), negative FC with a right superior/middle frontal gyrus cluster, and negative FC with a right superior lateral occipital cortex cluster. One difference was what appeared to be a slight anterior shift in FC for the R aI/fO seed relative to the right supramarginal gyrus or right central operculum seeds, which was particularly evident by the more anterior aspects of bilateral insula/frontoparietal operculum and ACC to which the R aI/fO was functionally connected.

To quantitatively compare these FC maps, we correlated the unthresholded, sample-averaged FC maps of the ROIs across all 187,410 in-mask brain voxels. This analysis revealed substantial similarity among FC maps. This was particularly true for the right central operculum and right supramarginal gyrus clusters, for which FC maps correlated across voxels at $r(187{,}408)$=.83, $p < 10^{-9}$. FC maps for the right central operculum and R aI/fO were correlated at $r(187{,}408)$ =.54, $p < 10^{-9}$. Finally, FC maps for the right supramarginal gyrus and

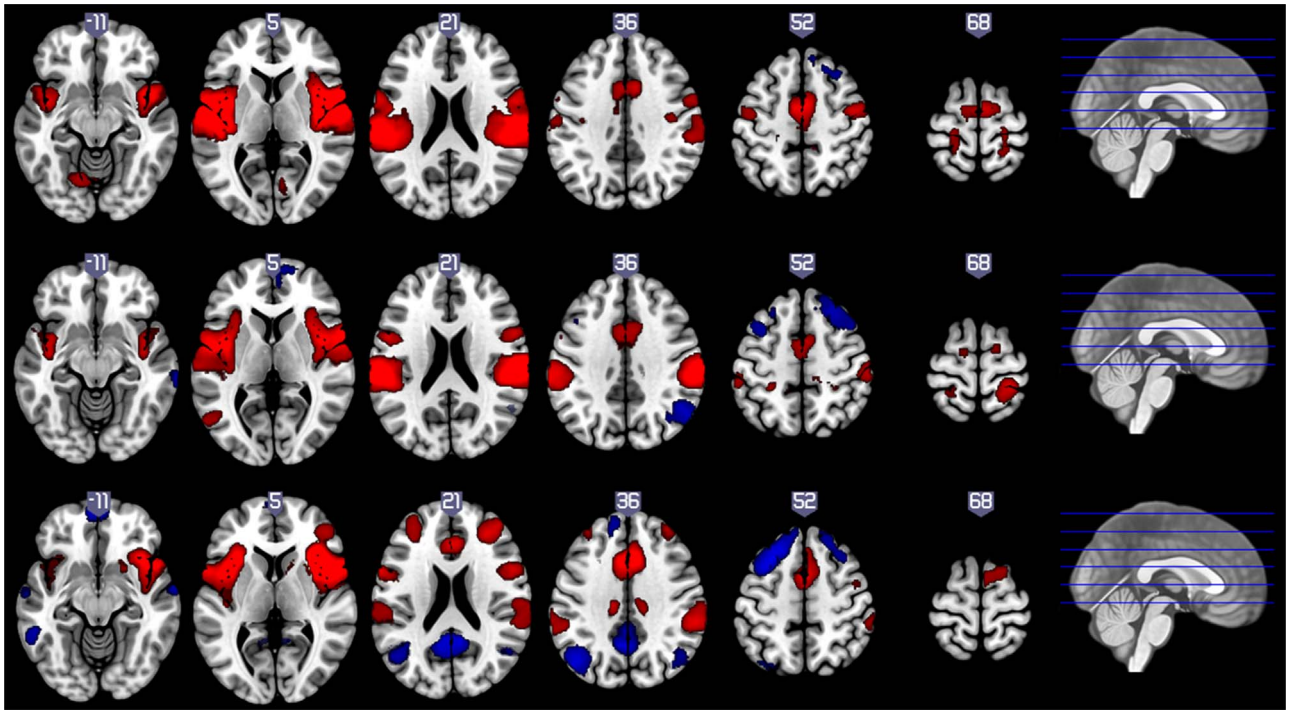

Fig. 3. Average functional connectivity (FC) maps between ROIs and the rest of the brain (height: p-uncorrected $< 10^{-8}$; cluster/extent: p-FWE $< 5 \cdot 10^{-6}$) shown in horizontal/axial brain slices. Top: FC map for the right central operculum cluster; Middle: FC map for the right supramarginal gyrus cluster; Bottom: FC map for the right anterior insula/frontal operculum (R aI/fO) ROI (Dosenbach et al., 2006). Red denotes positive, and blue denotes negative functional connectivity. MNI coordinates of slice depth (i.e., z-dimension) are, from left to right: [z=−11, +5, +21, +36, +52, and +68]. Information regarding the anatomical overlap of the clusters displayed, number of voxels per cluster, and peak coordinates can be found in Table 2A–C. Visualization was performed using MRIcroGL (http://www.cabiatl.com/mricrogl/).

Table 2
FC map anatomical overlap.

A. Right Central Operculum FC Map

Main Anatomical Region	# Voxels	MNI Peak
R Insula/Frontoparietal Operculum	7621	+54, +0, +2
L Insula/Frontoparietal Operculum	6463	−54, −6, +6
ACC/Medial SMA	2466	+4, −6, +60
L Lingual Gyrus	572	−10, −68, −8
L Postcentral Gyrus	300	−20, −32, +58
L Precentral Gyrus	295	−44, −10, +54
R Postcentral Gyrus	247	+22, −28, +70
R Middle/Superior Frontal Gyrus	131	+16, +32, +58
R Frontal Pole	71	+8, +32, +50

B. Right Supramarginal Gyrus FC Map

Main Anatomical Region	# Voxels	MNI Peak
R Insula/Frontoparietal Operculum	6192	+62, −22, +26
L Insula/Frontoparietal Operculum	5972	−62, −24, +24
ACC/Medial SMA	1735	+4, +0, +42
R Middle/Superior Frontal Gyrus	978	+34, +14, +44
R Superior Lateral Occipital Cortex	794	+50, −66, +44
R Postcentral Gyrus	655	+26, −36, +68
R Posterior Middle Temporal Gyrus	407	+60, −6, −28
L Middle Frontal Gyrus	327	−36, +6, +52
R Frontal Pole	238	+4, +50, +6
L Postcentral Gyrus	235	−26, −42, +64

C. Right Anterior Insula/Frontal Operculum FC Map

Main Anatomical Region	# Voxels	MNI Peak
R Insula/Frontoparietal Operculum	5334	+40, +16, +2
ACC/Medial SMA	3138	+6, +20, +36
L Insula/Frontoparietal Operculum	2628	−38, +16, +0
Precuneus	1951	−10, −50, +38
L Middle/Superior Frontal Gyrus	1692	−16, +42, +34
R Supramarginal Gyrus	1585	+60, −36, +40
L Superior Lateral Occipital Cortex	1348	−36, −78, +32
L Supramarginal Gyrus	909	−62, −22, +26
Bilateral Frontal Pole	829	+8, +62, −6
R Superior Lateral Occipital Cortex	648	+40, −60, +22

D. Combined R Central Operculum + R Supramarginal Gyrus FC Map

Main Anatomical Region	# Voxels	MNI Peak
R Insula/Frontoparietal Operculum	8192	+54, +0, +2
L Insula/Frontoparietal Operculum	7301	−60, −28, +22
ACC/Medial SMA	3630	+6, −4, +58
R Middle/Superior Frontal Gyrus	1289	+30, +14, +44
R Superior Lateral Occipital Cortex	767	+32, −74, +50
L Postcentral Gyrus	458	−24, −38, +64
R Posterior Middle Temporal Gyrus	243	+62, −20, −24
L Cerebellum 6/L Lingual Gyrus	189	−18, −66, −16
L Cerebellum 8	156	−32, −54, −60
L Inferior Lateral Occipital Cortex	119	−50, −66, +6

Note on 2D. These clusters were used as regions of interest (ROI) in subsequent ROI-to-ROI analyses.

Note. Tables display the ten largest regions of anatomical overlap, number of voxels, and peak MNI coordinates for each cluster used in functional connectivity mapping.

R aI/fO were correlated at $r(187{,}408)=.62$, $p < 10^{-9}$.

ROI-to-ROI connectivity results

We sought to elucidate which specific connections, within the network formed by combining thresholded FC maps for the right central operculum and right supramarginal gyrus (Table 2D, Fig. 4) were associated with PSI. A set of ten functional connections were associated with PSI (Figs. 5 and 6), when holding demographic and behavioral variables constant (all seed-level corrected at p-FDR $< .1$; uncorrected p-values are reported below): in subjects with higher PSI scores, the right central operculum cluster demonstrated increased FC to the right supramarginal gyrus cluster ($t(49)=2.59$, $p=.01$) (Fig. 6A), increased FC to the right insula/frontoparietal operculum ($t(49)=3.22$, $p=.002$) (Fig. 6B), increased FC to the left insula/frontoparietal operculum ($t(49)=2.44$, $p=.02$) (Fig. 6C), increased FC to the ACC/medial SMA ($t(49)=2.89$, $p=.006$) (Fig. 6D), reduced FC to the right middle/superior frontal gyrus cluster ($t(49)=-3.05$, $p=.004$) (Fig. 6E), and increased FC to the left postcentral gyrus ($t(49)=2.32$, $p=.02$) (Fig. 6F). The right middle/superior frontal gyrus also displayed decreased FC to the left insula/frontoparietal operculum in subjects with higher PSI scores ($t(49)=-3.24$, $p=.002$) (Fig. 6G). After adding the three main ROIs of the cingulo-opercular network (bilateral aI/fO and dACC/msFC; Dosenbach et al., 2006) to this network, higher PSI was additionally associated with reduced FC between the right middle/superior frontal gyrus and the left aI/fO ($t(49)=-2.78$, $p=.008$) (Fig. 6H). Finally, the left cerebellum 8 cluster exhibited increased FC to both the left postcentral gyrus ($t(49)=2.93$, $p=.005$) (Fig. 6I) and the left insula/frontoparietal operculum ($t(49)=2.69$, $p=.01$) (Fig. 6J). For the full networks of significant FC associations, see Fig. 5.

Ancillary analyses

Test for lateralization of functional connectivity associations

To statistically test for hemispheric lateralization of FC associations, we undertook a series of dependent correlation analyses. These analyses enabled us to distinguish between four possible scenarios: 1. lateralized effects which prove significantly stronger than those of the contralateral side, and in which contralateral effects are non-significant; 2. lateralized effects which prove significantly stronger than those of the contralateral side, but in which contralateral effects are also significant; 3. non-lateralized effects which are not significantly stronger than those of the contralateral side, and in which contralateral effects are significant; and 4. non-lateralized effects which are not significantly stronger than those of the contralateral side, and wherein contralateral effects are non-significant.

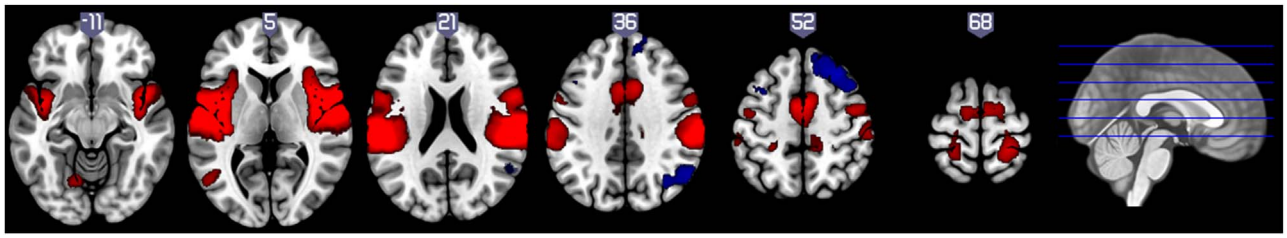

Fig. 4. Horizontal/axial brain slices displaying the average/combined functional connectivity (FC) map of the right central operculum and right supramarginal gyrus ICC clusters. (height: p-uncorrected $< 10^{-8}$, cluster/extent: p-FWE $5{\cdot}10^{-7}$). Red denotes positive, and blue denotes negative FC. MNI coordinates of slice depth (z-dimension) are, from left to right: [z=−11, +5, +21, +36, +52, and +68]. Information regarding the anatomical overlap of the clusters displayed, number of voxels per cluster, and peak coordinates can be found in Table 2D. Visualization was performed using MRIcroGL (http://www.cabiatl.com/mricrogl/).

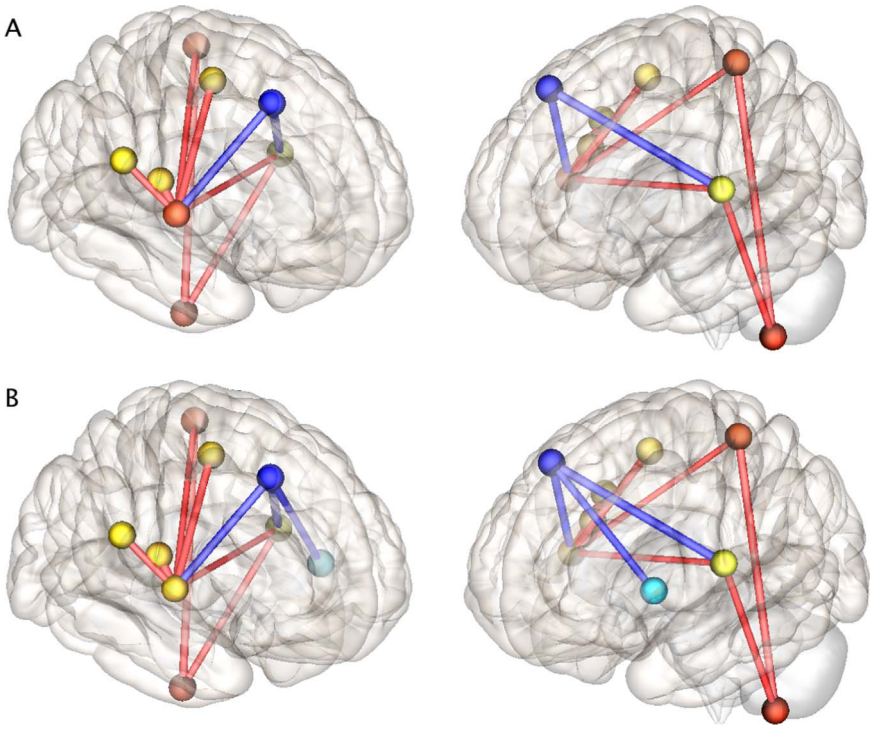

Fig. 5. ROI-to-ROI networks. **A**, right and left lateral views of a network which consists of the right central operculum, right supramarginal gyrus, and combined FC map clusters (Table 2D, Fig. 4). **B**, right and left lateral views of a network which consists of the right central operculum, right supramarginal gyrus, combined FC map clusters, and additionally, the bilateral anterior insula/frontal operculum (aI/fO) and dorsal anterior cingulate cortex of the cinguloopercular network (Dosenbach et al., 2006). Connection thickness is proportional to the *t*-statistic from the association between loneliness, controlling covariates, and strength of FC. Red connections denote that lonelier subjects have increased FC, and blue connections denote that lonelier subjects have reduced FC. Hot or cold ROI colors also correspond to magnitude of the association between network-average FC and loneliness, controlling for covariates. Scatter plots depicting the relationship between each connection displayed and loneliness scores are found in Fig. 6. This figure was rendered using custom settings within the "ROI second-level results, 3D Display" module of CONN Toolbox version 15c (Whitfield-Gabrieli and Nieto-Castanon, 2012).

For our main ICC results, we generated a set of homologous regions contralateral to the right central operculum and the right supramarginal gyrus. ICC scores were averaged across the voxels comprising each region, and these averages were correlated across-subjects with PSI scores. We also correlated the average ICC scores of the original right central operculum and right supramarginal gyrus clusters with R-UCLA scores. Steiger's Z-tests (Steiger, 1980) were implemented to test whether the average ICC scores of right-hemispheric regions showed significantly stronger associations with PSI than the corresponding left-hemispheric regions.

Results revealed that the average ICC scores of the right central operculum were significantly more correlated with PSI than those of the left central operculum (Steiger's Z=2.40, $p < 0.01$), but the ICC of the left central operculum was also significantly correlated with PSI (r(53)=.36, p=.01). Thus, the central operculum cluster fit scenario two, as described above. Average ICC scores of the right supramarginal gyrus were also significantly more correlated with PSI than those of the left supramarginal gyrus (Steiger's Z=2.66, $p < 0.005$). In this case, however, average ICC scores of the left supramarginal gyrus were only marginally correlated with PSI (r(53)=.22, p=.10). Thus, the supramarginal gyrus better fit scenario one. Based upon these results, our main ICC results appear to be primarily right-lateralized, although a smaller significant effect was also found in the left central operculum.

Although results from ROI-to-ROI analyses appeared to be more bilaterally distributed than ICC results, one aspect of these results in particular – associations observed for the right middle/superior frontal gyrus – appeared to be putatively right-lateralized. Thus, we undertook a similar analysis to test for lateralization of these results: A homologous ROI to the right middle/superior frontal gyrus was generated in the left hemisphere. Next, the average signal across the voxels of this ROI was extracted. Then, Fisher's z-transformed correlations were computed between these signals and the average signal of ROIs wherein FC with the right middle/superior frontal was associated with PSI in ROI-to-ROI analyses (the right central operculum, the L insula/frontoparietal operculum, and the L aI/fO). Here, we adjusted PSI scores for age, gender, CES-D-ML scores, and isolation, to assure the specificity of results for PSI, and to be consistent with ROI-to-ROI analyses.

These analyses revealed that FC between the left middle/superior frontal gyrus and right central operculum was only marginally related to PSI (r(53)=−.24, p=.08). FC shared between the left middle/superior frontal gyrus and L insula/frontoparietal operculum (r(53)=−.21, $p > .1$), as well as between the left middle/superior frontal gyrus and L aI/fO (r(53)=−.18, $p > .15$), was non-significantly related to PSI. Steiger's Z-tests revealed that the association between PSI, controlling covariates, and right middle/superior frontal gyrus FC to right central operculum (Steiger's Z=−1.12, p=.13) was non-significant, to L insula/frontoparietal operculum (Steiger's Z=−1.36, p=.09) was marginally significant, and to L aI/fO (Steiger's Z=−1.16, p=.12) was non-significant. These results, with some effects marginally greater in the right hemisphere and some effects marginally significant in the left hemisphere, do not cleanly fit within a single category outlined above and therefore do not strongly support lateralization of the middle/superior frontal gyrus FC effects.

The effect of objective social isolation on brain-wide functional connectivity

The central aim of this study has been to characterize functional brain networks associated specifically with PSI, a measure which tends to only minimally correlate with objective social isolation (Holt-Lunstad et al., 2015; Steptoe et al., 2013). However, objective social isolation is also researched for its effects on brain structure and function (e.g., Liu et al., 2012; Makinodan et al., 2012), and it is

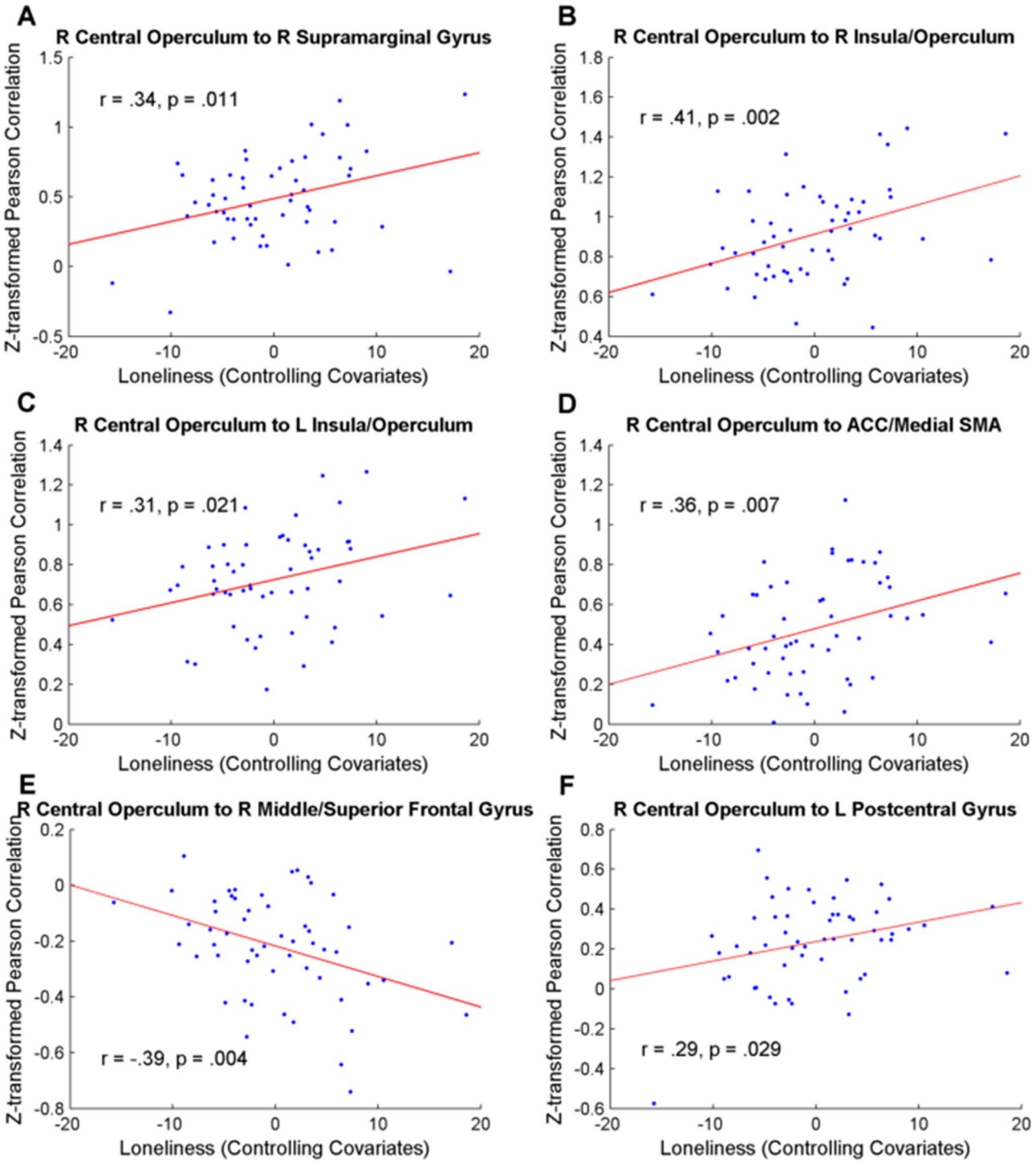

Fig. 6. Scatter plots of UCLA loneliness scores, statistically controlling for covariates, (x-axis) plotted against Fisher's z-transformed Pearson correlations (i.e., functional connectivity) between the average time series of each pair of ROIs listed in each title (y-axis; network shown in Fig. 5). Raw correlations and uncorrected p-values are displayed for the across subjects association between loneliness scores (R-UCLA) and ROI-to-ROI functional connectivity (FC). Least-squares trend lines are displayed to highlight approximate relationships. A, R-UCLA scores versus FC between the right central operculum and right supramarginal gyrus (both clusters obtained via main ICC analysis). B, R-UCLA scores versus FC between the right central operculum and right insula/frontoparietal operculum (latter cluster obtained via FC mapping; see Table 2D, Fig. 4). C, R-UCLA scores versus FC between the right central operculum and left insula/frontoparietal operculum (latter cluster obtained via FC mapping). D, R-UCLA scores versus FC between the right central operculum and the anterior cingulate cortex/medial supplementary motor area (ACC/Medial SMA; latter cluster obtained via FC mapping). E, R-UCLA scores versus FC between the right central operculum and the right middle/superior frontal gyrus (latter cluster obtained via FC mapping). F, R-UCLA scores versus FC between the right central operculum and the left postcentral gyrus (latter cluster obtained via FC mapping). G, R-UCLA scores versus FC between the right middle/superior frontal gyrus and left insula/frontoparietal operculum. H, R-UCLA scores versus FC between the right central operculum and left anterior insula/frontal operculum (L aI/fO; this latter cluster was obtained using the peak coordinates reported by Dosenbach et al. (2006)). I, R-UCLA scores versus FC between the left cerebellum region 8 and the left postcentral gyrus (both clusters obtained via FC mapping). J, R-UCLA scores versus FC between the left insula/frontoparietal operculum and left cerebellum region 8. This figure was created using custom Matlab 2014a (Mathworks, Inc., Nattick, MA) scripts.,

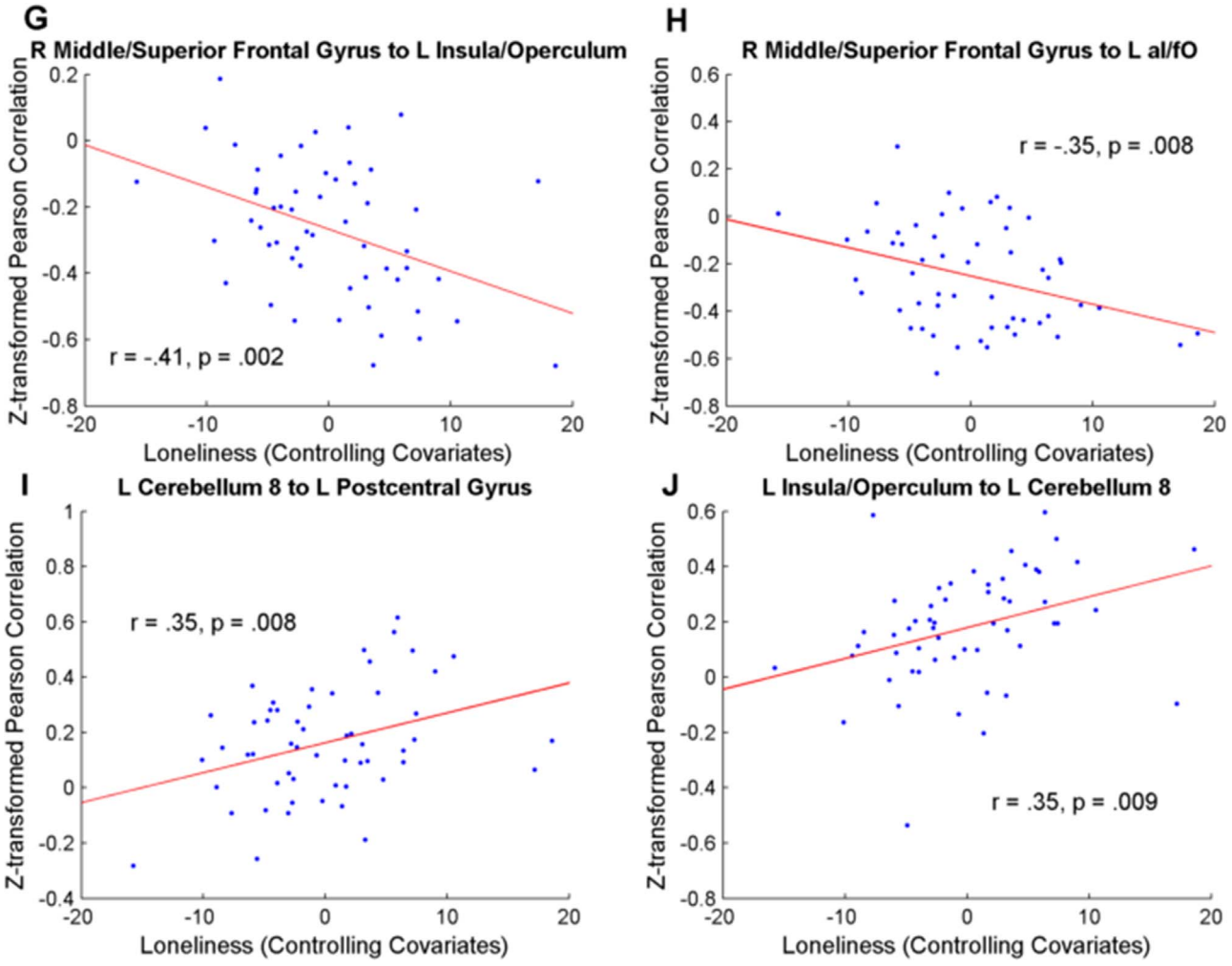

Fig. 6. (*continued*)

thought to exert independent effects from PSI on morbidity and mortality (Holt-Lunstad et al., 2015). Therefore, we considered that it would be beneficial to conduct a follow-up analysis for the effect of objective social isolation on brain-wide ICC. We performed a brain-wide search for clusters of voxels showing a significant association between ICC and objective social isolation, using the same thresholds as for our main analyses concerning loneliness (primary threshold: p-uncorrected < .005, cluster-extent threshold: p-FWE < .05) in CONN Toolbox. We detected no significant clusters of brain voxels related to objective isolation in this two-tailed bivariate contrast, or in a two-tailed contrast controlling for loneliness.

Addition of the bilateral amygdala, subgenual cingulate, bilateral lingual gyrus, and posterior cingulate cortex to ROI-to-ROI analyses

Evidence consistently suggests the involvement of the subgenual cingulate in mood disorders such as depression (Drevets et al., 2008; Greicius et al., 2007; Johansen-Berg et al., 2008), and the involvement of the amygdala in attachment insecurity (Lemche et al., 2006; Vrtička et al., 2008). Moderate positive associations between PSI and depressive symptomatology are consistently identified, wherein PSI consistently predicts depressive symptomatology longitudinally but not vice versa (e.g., Cacioppo et al., 2006). Additionally, high attachment ambivalence, low attachment security, and attachment anxiety have all shown moderate correlations with PSI in prior studies (Wei et al., 2005; Wiseman et al., 2006). Therefore, to investigate possible interrelations among brain networks underlying depressive symptomatology, attachment insecurity, and PSI, we sought to include these ROIs in an additional ROI-to-ROI analysis. Based on recent findings by Lan et al. (2015), we also included a bilateral lingual gyrus ROI in this network. Insights gleaned from this analysis could potentially prove useful and informative for future investigations.

We obtained an ROI for the subgenual cingulate by creating a 4 mm radius spherical ROI centered on the peak coordinate (MNI: −10, +5, −10) reported by Greicius et al. (2007). We obtained bilateral amygdala ROIs from the FSL Harvard-Oxford atlas. We chose to include both the left and right amygdala based on prior work showing bilateral effects for attachment styles (e.g., Lemche et al., 2006). Additionally, we obtained a 4 mm radius bilateral lingual gyrus ROI from coordinates reported by Lan et al. (2015) (MNI: −9, −81, +3). These four ROIs were added to an ROI-to-ROI network also containing FC mapping ROIs detailed in Table 2D, as well as the right central operculum and right supramarginal gyrus clusters.

We first investigated bivariate associations between functional connections in this network and PSI. This analysis revealed two associations not noted previously: the left amygdala showed reduced FC to the right middle frontal gyrus in lonelier subjects ($t(53)=-3.04$, p-FDR=.033), and the right amygdala also showed a non-significant trend toward reduced FC to this ROI ($t(53)=-2.46$, p-FDR=.078). Second, we repeated this analysis controlling for depressive symptomatology, objective social isolation, age, and gender. In this case, the association between PSI and right amygdala to right supramarginal gyrus FC was non-significant ($t(49)=-1.58$, p-FDR > .24), whereas the association between PSI and FC between the left amygdala and right

middle frontal gyrus remained significant ($t(49)=-2.9$, p-FDR=.033). The only other trend not previously noted was a non-significant association of PSI with reduced FC between the subgenual cingulate and dorsal ACC ($t(49)=-2.9$, p-FDR=.085), which was previously non-significant in the bivariate comparison ($t(49)=-2.27$, p-FDR > .16). No additional significant associations were observed which were not reported previously in "ROI-to-ROI Connectivity Results" and shown in Figs. 5 and 6.

Discussion

This study provided the first evidence for an association between PSI and functional brain connectivity in a sample of healthy young adults. Importantly, the FC features observed here do not represent task-evoked responses but rather reflect neural predispositions associated with PSI, as gauged by resting-state FC. We hypothesized that participants higher in PSI would demonstrate altered FC within brain networks underlying attention, such as the cingulo-opercular network, the VAN, or the dorsal attention network (Corbetta and Shulman, 2002). Our results suggest that PSI is characterized by increased brain-wide FC in the right central operculum and right supramarginal gyrus, and that these associations are not mediated by depressive symptomatology, objective isolation, age, or gender. FC in the right central operculum and right supramarginal gyrus explained a combined 36% of variance in PSI in our sample, and ancillary analyses supported the notion that these were primarily right-lateralized effects. The right supramarginal gyrus cluster was not identified in a subsequent brain-wide multiple regression controlling for behavioral and demographic covariates, but this was likely due to an overcorrection, given (a) the moderately high correlation between PSI and depressive symptomatology, and (b) mediation analyses indicated that depressive symptomatology did not mediate the association between PSI and right supramarginal gyrus FC. However, right central operculum ICC did significantly mediate the association between right supramarginal gyrus FC and PSI. This and FC mapping analyses suggest that these clusters represent two closely associated elements within a broader network.

PSI and increased functional connectivity within the cingulo-opercular network

We further explicated our results by computing seed-based FC maps for each cluster identified in main analyses. These revealed associations between PSI and FC in a distributed network, which included the right middle/superior frontal gyrus, bilateral insula/frontoparietal opercula, ACC/pre-SMA, left cerebellum, and left post-central gyrus. The right central operculum and right supramarginal gyrus regions, as well as the bilateral insula/frontoparietal operculum and ACC/pre-SMA regions identified by FC mapping, coincided well with regions of the cingulo-opercular network (Dosenbach et al., 2006; Power et al., 2011). This connection was further supported by correlations between the FC maps of the right supramarginal gyrus and right central operculum clusters and the FC map of the R aI/fO, a region consistently identified as a key hub of the cingulo-opercular network (Dosenbach et al., 2006; Dosenbach et al., 2007; Eckert et al., 2009; Sridharan et al., 2008). Notably, multiple key regions of the cingulo-opercular network showed increased FC as a function of PSI, including the right central operculum and ACC/pre-SMA, the right central operculum and left insula/frontoparietal operculum, the right central operculum and right supramarginal gyrus, and the right central operculum to a broader area of right insula/frontoparietal operculum.

The cingulo-opercular network has been implicated in at least three distinct but non-mutually exclusive processing functions, including stable maintenance of task sets (Dosenbach et al., 2006, 2007), salience encoding (Seeley et al., 2007), and maintenance of tonic alertness, a cognitive construct distinct from physiological arousal (Sadaghiani and D'Esposito, 2015; Sadaghiani et al., 2010). Sadaghiani and D'Esposito (2014) argued that a generalized role in sustaining tonic alertness may underlie the more specialized role in task set maintenance, as sustained alertness signals are a prerequisite for maintaining attention during tasks. Additionally, Sadaghiani and D'Esposito (2015) noted that the specific region of anterior insula thought to encode salience (Seeley et al., 2007) also proved important for maintaining tonic alertness and was not differentiated from other regions of the aI/fO in this regard. Thus, maintenance of tonic alertness may help to integrate these various functional roles of the cingulo-opercular network into a unified framework.

The association between PSI and the cingulo-opercular network is consistent with the notion that a heightened tonic alertness subserves individuals' implicit vigilance for social threats in PSI. Notably, we observed a pattern of increased cingulo-opercular within-network connectivity in PSI, a connectivity signature characteristic of elevated tonic alertness (Sadaghiani and D'Esposito, 2015). Heightened tonic alertness, particularly if geared specifically toward social stimuli, could help to explain why individuals experiencing PSI display increased gaze fixations on negative social scenes (Bangee et al., 2014; Qualter et al., 2013) and process negative social information more quickly (S. Cacioppo et al., 2015; S. Cacioppo et al., 2015). However, an alternative explanation is that increased cingulo-opercular FC in PSI may represent maintenance of mental task sets involved in the processing of (often negative) social information and/or greater personal salience accorded to such processing.

Notably, the brain regions identified in our study may also be related to physiological findings associated with PSI, including sleep fragmentation, elevated basal levels of vascular resistance, and HPA activation. Parts of the insula, frontoparietal operculum, and ACC/pre-SMA identified in our analyses have been associated with regulation of sympathetic arousal by the autonomic nervous system (Abboud et al., 2006; Beissner et al., 2013; Eckert et al., 2009; Meyer et al., 2004). Regulation of tonic alertness by the cingulo-opercular network may act independently of autonomic arousal mechanisms, instead relying upon inhibitory control involving global field power in the upper alpha band (Sadaghiani and D'Esposito, 2015; Sadaghiani et al., 2010, 2012), but this does not discount the possibility that these same brain regions may subserve multiple distinct processing functions.

PSI and dysconnection between the frontoparietal and cingulo-opercular networks

Another aspect of our results, reduced FC between right middle/superior frontal gyrus and several regions of the cingulo-opercular network, suggests that up-regulated tonic alertness for social threat detection may sap vital resources necessary for the successful engagement of executive control processes. The right middle/superior frontal gyrus cluster identified by FC mapping analyses (Table 2D, Fig. 4) spatially overlapped a region commonly labelled as the right dorsolateral prefrontal cortex (R DLPFC) in previous studies (e.g., MNI coordinates, +42, +14, +32, in Etkin et al., 2006; MNI coordinates, +45, +16, +45, in Sridharan et al., 2008). The R DLPFC is a component of the frontoparietal executive control network (Petersen and Posner, 2012; Sridharan et al., 2008), which plays important roles in conflict and interference resolution (Etkin et al., 2006; Nee et al., 2007; Petersen and Posner, 2012; Ruz and Tudela, 2011) and prepotent response inhibition (Simmonds et al., 2008; Swick et al., 2011). The cingulo-opercular network and frontoparietal networks share minimal or negative FC at rest (Dosenbach et al., 2007; Nelson et al., 2010; Sadaghiani and D'Esposito, 2015; Seeley et al., 2007). However, between-network connectivity increases rapidly upon engagement in difficult or attention-demanding tasks (Sadaghiani and D'Esposito, 2015). Based upon Granger causality analysis, the direction of information flow primarily proceeds from the R aI/fO to the R DLPFC, both at rest and during tasks (Sridharan et al., 2008). Furthermore, the R aI/fO may enable switching between the default mode and frontopar-

ietal networks at the onset of tasks via entrainment of the R DLPFC and frontoparietal network (Sridharan et al., 2008). Thus, reduced FC between the right middle/superior frontal gyrus and regions of the cingulo-opercular network in PSI may imply a reduced ability to engage executive control processes at the onset of tasks. This insight may help explain previous findings such as high-PSI individuals' reduced ability to inhibit prepotent responding in a dichotic listening task (Cacioppo et al., 2000; see also Baumeister et al., 2005).

Alternative interpretations

Although our interpretation of results has focused on the notion of the cingulo-opercular network as a key mechanism for implicit attentional processing, there is also significant evidence linking the right central operculum to emotional processing. Lesion case studies have reported frontoparietal opercular lesions resulting in loss of the ability to create facial expressions of emotion, whereas other voluntary facial movements remained intact (Campello et al., 1994; Sim et al., 2005). Additionally, regions of the right frontoparietal operculum have been linked to emotional prosody detection and processing using fMRI (Kotz et al., 2003), transcranial magnetic stimulation (Hoekert et al., 2008; Van Rijn et al., 2005), and lesion mapping (Adolphs et al., 2002). Interestingly, these studies have primarily indicated associations between the frontoparietal operculum and prosodic expressions specific to withdrawal emotions (fear and sadness). This may present a congruent pattern to the association between PSI and cognitive attunement to negative or threatening social stimuli. Notably, a role for the right central operculum cluster in emotional processing functions does not necessarily stand in contrast with interpretations involving the cingulo-opercular network. For instance, it seems plausible that more central and posterior aspects of insula/frontoparietal operculum may be particularly involved in cingulo-opercular functions pertaining to affective processing, including threat processing. This interpretation is at least partially supported by meta-analyses of insula function (Kurth et al., 2010) and emotion processing (Kober et al., 2008), which demonstrated a partial anterior-posterior trend: cognitive and attention processing preferentially involved frontal aspects of insula/frontoparietal operculum, whereas emotion-related processing preferentially involved more central and posterior aspects of insula/frontoparietal operculum.

Our main findings involving the right central operculum and right supramarginal gyrus clusters might also be considered suggestive of altered somatosensation in PSI. For instance, Keysers et al. (2010) noted that parts of the frontoparietal operculum contain secondary somatosensory cortex (SII) somatotopic regions, and that these may be involved in social perception. Additionally, the junction between the right supramarginal gyrus and angular gyrus (MNI peak: +58, −46, +10) is thought to be involved in integrating somatosensory and vestibular body orientation information (De Ridder et al., 2007). We noted, however, that over 60% of the voxels of the right central operculum cluster identified resided within the central opercular cortex, as defined by the Harvard-Oxford atlas, and no voxels resided within the parietal opercular cortex. It is the parietal operculum which is most often associated with somatosensation (Eickhoff et al., 2010), whereas less consistent associations have been observed for frontal and central opercula (Baumgärtner et al., 2010). We also noted that the right supramarginal gyrus cluster identified was largely anterior and superior to the supramarginal-angular gyrus junction region identified by De Ridder et al. (2007). Therefore, although we do not rule out interpretations involving altered somatosensation, we believe that these are less plausible than cognitive or emotional processing interpretations, given the anatomical overlap of clusters identified.

Limitations

Although our findings are consistent with the notion that the cingulo-opercular network and tonic alertness may underlie the implicit hypervigilance to social threat that characterizes PSI, and that reduced FC between the frontoparietal and cingulo-opercular network may underlie executive dysfunction in PSI, these postulates must be left for future studies to confirm using behavioral tasks. As prior studies indicate that these cognitive phenomena are largely implicit (S. Cacioppo et al., 2015; S. Cacioppo et al., 2015), behavioral tasks such as the social Stroop will likely be required for this purpose, rather than self-report measures. Additionally, in this study we did not have access to ratings of time-sensitive *state* PSI measured during the scanning session. The UCLA scale, a measure of *trait* PSI, is known to be highly stable across time (Russell, 1996; Sarason et al., 1986) and correlates moderately with state PSI in experience sampling studies (van Roekel et al., 2016). However, separate ratings of state PSI might offer additional statistical power for future neuroimaging studies. Finally, we did not have access to semi-structured interview measures of PSI or depressive symptomatology in this study. Although the UCLA scale is likely the most widely used measure of PSI (Austin, 1983; McWhirter, 1990), interview techniques could potentially offer a more detailed, subject-specific picture of these variables in future studies.

Conclusion

Overall, our results suggest a crucial role for the cingulo-opercular network in PSI, due to (a) high correlations between FC maps; (b) associations between PSI and increased FC among several cingulo-opercular regions; and (c) decreased connectivity between a key hub of this network (the left aI/fO) and the right middle/superior frontal gyrus, directly paralleling results obtained for our more posterior right central operculum cluster. Future investigations will be needed to elucidate to what extent emotional processing interpretations fit within the context of cingulo-opercular network interpretations, how specific cingulo-opercular functions may be related to hypervigilance for social threat, and whether decreased FC between cingulo-opercular and frontoparietal network nodes underlies selective executive dysfunction in PSI. Our hope is that the current study lays a groundwork for such investigations.

Conflicts of interest

The authors declare no competing financial interests.

Acknowledgements

This work was supported by a MIUR grant (PRIN 2010XPMFW4_008; I meccanismi neurocognitivi alla base delle interazioni sociali) to Stefano F. Cappa.

Appendix A. Supplementary material

Supplementary data associated with this article can be found in the online version at http://dx.doi.org/10.1016/j.neuroimage.2016.09.050.

References

Abboud, H., Berroir, S., Labreuche, J., Orjuela, K., Amarenco, P., 2006. Insular involvement in brain infarction increases risk for cardiac arrhythmia and death. Ann. Neurol. 59 (4), 691–699.
Adolphs, R., Damasio, H., Tranel, D., 2002. Neural systems for recognition of emotional prosody: a 3-D lesion study. Emotion 2 (1), 23.
Anticevic, A., Hu, S., Zhang, S., Savic, A., Billingslea, E., Wasylink, S., Krystal, J.H., 2014. Global resting-state functional magnetic resonance imaging analysis identifies frontal cortex, striatal, and cerebellar dysconnectivity in obsessive-compulsive disorder. Biol. Psychiatry 75 (8), 595–605.
Austin, B.A., 1983. Factorial structure of the UCLA loneliness scale. Psychol. Rep. 53 (3), 883–889.
Bangee, M., Harris, R.A., Bridges, N., Rotenberg, K.J., Qualter, P., 2014. Loneliness and

attention to social threat in young adults: Findings from an eye tracker study. Pers. Individ. Differ. 63, 16–23.
Baumeister, R.F., DeWall, C.N., Ciarocco, N.J., Twenge, J.M., 2005. Social exclusion impairs self-regulation. J. Pers. Social. Psychol. 88 (4), 589.
Baumgärtner, U., Iannetti, G.D., Zambreanu, L., Stoeter, P., Treede, R.D., Tracey, I., 2010. Multiple somatotopic representations of heat and mechanical pain in the operculo-insular cortex: a high-resolution fMRI study. J. Neurophysiol. 104 (5), 2863–2872.
Behzadi, Y., Restom, K., Liau, J., Liu, T.T., 2007. A component based noise correction method (CompCor) for BOLD and perfusion based fMRI. NeuroImage 37 (1), 90–101.
Beissner, F., Meissner, K., Bär, K.-J., Napadow, V., 2013. The autonomic brain: an activation likelihood estimation meta-analysis for central processing of autonomic function. J. Neurosci. 33 (25), 10503–10511.
Buckner, R.L., Sepulcre, J., Talukdar, T., Krienen, F.M., Liu, H., Hedden, T., Johnson, K.A., 2009. Cortical hubs revealed by intrinsic functional connectivity: mapping, assessment of stability, and relation to Alzheimer's disease. J. Neurosci. 29 (6), 1860–1873.
Cacioppo, J.T., Patrick, W., 2008. Loneliness: Human Nature and the Need for Social Connection. WW Norton & Company.
Cacioppo, J.T., Hawkley, L.C., 2009. Perceived social isolation and cognition. Trends Cogn. Sci. *13* (10), 447–454.
Cacioppo, J.T., Hawkley, L.C., Thisted, R.A., 2010. Perceived social isolation makes me sad: 5-year cross-lagged analyses of loneliness and depressive symptomatology in the Chicago Health, Aging, and Social Relations Study. Psychol. Aging 25 (2), 453.
Cacioppo, J.T., Cacioppo, S., Boomsma, D.I., 2014. Evolutionary mechanisms for loneliness. Cogn. Emot. 28 (1), 3–21.
Cacioppo, J.T., Cacioppo, S., Capitanio, J.P., Cole, S.W., 2015. The neuroendocrinology of social isolation. Annu. Rev. Psychol. 66, 733–767. http://dx.doi.org/10.1146/annurev-psych-010814-015240.
Cacioppo, J.T., Hughes, M.E., Waite, L.J., Hawkley, L.C., Thisted, R.A., 2006. Loneliness as a specific risk factor for depressive symptoms: cross-sectional and longitudinal analyses. Psychol. Aging 21 (1), 140.
Cacioppo, J.T., Norris, C.J., Decety, J., Monteleone, G., Nusbaum, H., 2009. In the eye of the beholder: individual differences in perceived social isolation predict regional brain activation to social stimuli. J. Cogn. Neurosci. 21 (1), 83–92.
Cacioppo, J.T., Ernst, J.M., Burleson, M.H., McClintock, M.K., Malarkey, W.B., Hawkley, L.C., Hugdahl, K., 2000. Lonely traits and concomitant physiological processes: the MacArthur social neuroscience studies. Int. J. Psychophysiol. 35 (2), 143–154.
Cacioppo, J.T., Hawkley, L.C., Crawford, L.E., Ernst, J.M., Burleson, M.H., Kowalewski, R.B., Berntson, G.G., 2002. Loneliness and health: potential mechanisms. Psychosom. Med. 64 (3), 407–417.
Cacioppo, J.T., Hawkley, L.C., Ernst, J.M., Burleson, M., Berntson, G.G., Nouriani, B., Spiegel, D., 2006. Loneliness within a nomological net: an evolutionary perspective. J. Res. Pers. 40 (6), 1054–1085.
Cacioppo, S., Cacioppo, J.T., 2016. Research in social neuroscience: how perceived social isolation, ostracism, and romantic rejection affect your brain. In: Riva, P., Eck, J. (Eds.), Social Exclusion. Springer International Publishing, Switzerland, 73–88. http://dx.doi.org/10.1007/978-3-319-33033-4_4.
Cacioppo, S., Capitanio, J.P., Cacioppo, J.T., 2014. Toward a neurology of loneliness. Psychol. Bull. 140 (6), 1464. http://dx.doi.org/10.1037/a0037618.
Cacioppo, S., Balogh, S., Cacioppo, J.T., 2015. Implicit attention to negative social, in contrast to nonsocial, words in the Stroop task differs between individuals high and low in loneliness: evidence from event-related brain microstates. Cortex 70, 213–233.
Cacioppo, S., Grippo, A.J., London, S., Goossens, L., Cacioppo, J.T., 2015. Loneliness clinical import and interventions. Perspect. Psychol. Sci. 10 (2), 238–249.
Cacioppo, S., Bangee, M., Balogh, S., Cardenas-Iniguez, C., Qualter, P., Cacioppo, J.T., 2015. Loneliness and implicit attention to social threat: a high-performance electrical neuroimaging study. Cogn. Neurosci., 1–22.
Campello, I., Velilla, I., López-López, A., Tapiador, M., Marta, E., Martín-Martínez, J., 1994. Biopercular lesion with inverse dissociation. Rev. Neurol. 23 (123), 1056–1058.
Cole, M.W., Pathak, S., Schneider, W., 2010. Identifying the brain's most globally connected regions. NeuroImage 49 (4), 3132–3148.
Corbetta, M., Shulman, G.L., 2002. Control of goal-directed and stimulus-driven attention in the brain. Nat. Rev. Neurosci. 3 (3), 201–215.
Dai, Z., Yan, C., Li, K., Wang, Z., Wang, J., Cao, M., Bi, Y., 2014. Identifying and mapping connectivity patterns of brain network hubs in Alzheimer's disease. Cereb. Cortex, 46 , bhu246.
De Ridder, D., Van Laere, K., Dupont, P., Menovsky, T., Van de Heyning, P., 2007. Visualizing out-of-body experience in the brain. N. Engl. J. Med. 357 (18), 1829–1833.
Dosenbach, N.U., Visscher, K.M., Palmer, E.D., Miezin, F.M., Wenger, K.K., Kang, H.C., Petersen, S.E., 2006. A core system for the implementation of task sets. Neuron 50 (5), 799–812.
Dosenbach, N.U., Fair, D.A., Miezin, F.M., Cohen, A.L., Wenger, K.K., Dosenbach, R.A., Raichle, M.E., 2007. Distinct brain networks for adaptive and stable task control in humans. Proc. Natl. Acad. Sci. 104 (26), 11073–11078.
Drevets, W.C., Savitz, J., Trimble, M., 2008. The subgenual anterior cingulate cortex in mood disorders. CNS Spectr. 13 (8), 663.
Dukart, J., Bertolino, A., 2014. When structure affects function–the need for partial volume effect correction in functional and resting state magnetic resonance imaging studies. PLoS One 9 (12), e114227.
Eckert, M.A., Menon, V., Walczak, A., Ahlstrom, J., Denslow, S., Horwitz, A., Dubno, J.R., 2009. At the heart of the ventral attention system: the right anterior insula. Hum. Brain Mapp. 30 (8), 2530–2541.
Eickhoff, S.B., Jbabdi, S., Caspers, S., Laird, A.R., Fox, P.T., Zilles, K., Behrens, T.E., 2010. Anatomical and functional connectivity of cytoarchitectonic areas within the human parietal operculum. J. Neurosci. 30 (18), 6409–6421.
Etkin, A., Egner, T., Peraza, D.M., Kandel, E.R., Hirsch, J., 2006. Resolving emotional conflict: a role for the rostral anterior cingulate cortex in modulating activity in the amygdala. Neuron 51 (6), 871–882.
Evans, T.M., Kochalka, J., Ngoon, T.J., Wu, S.S., Qin, S., Battista, C., Menon, V., 2015. Brain structural integrity and intrinsic functional connectivity forecast 6 year longitudinal growth in children's numerical abilities. J. Neurosci. 35 (33), 11743–11750.
Friston, K.J., Ashburner, J., Frith, C.D., Poline, J.-B., Heather, J.D., Frackowiak, R.S., 1995. Spatial registration and normalization of images. Hum. Brain Mapp. 3 (3), 165–189.
Greicius, M.D., Flores, B.H., Menon, V., Glover, G.H., Solvason, H.B., Kenna, H., Schatzberg, A.F., 2007. Resting-state functional connectivity in major depression: abnormally increased contributions from subgenual cingulate cortex and thalamus. Biol. Psychiatry 62 (5), 429–437.
Hallquist, M.N., Hwang, K., Luna, B., 2013. The nuisance of nuisance regression: spectral misspecification in a common approach to resting-state fMRI preprocessing reintroduces noise and obscures functional connectivity. NeuroImage 82, 208–225.
Hayasaka, S., Phan, K.L., Liberzon, I., Worsley, K.J., Nichols, T.E., 2004. Nonstationary cluster-size inference with random field and permutation methods. NeuroImage 22 (2), 676–687.
Hoekert, M., Bais, L., Kahn, R.S., Aleman, A., 2008. Time course of the involvement of the right anterior superior temporal gyrus and the right fronto-parietal operculum in emotional prosody perception. PLoS One 3 (5), e2244.
Holt-Lunstad, J., Smith, T.B., Baker, M., Harris, T., Stephenson, D., 2015. Loneliness and social isolation as risk factors for mortality: a meta-analytic review. Perspect. Psychol. Sci. 10 (2), 227–237.
Holwerda, T.J., Deeg, D.J., Beekman, A.T., van Tilburg, T.G., Stek, M.L., Jonker, C., Schoevers, R.A., 2014. Feelings of loneliness, but not social isolation, predict dementia onset: results from the Amsterdam Study of the Elderly (AMSTEL). J. Neurol. Neurosurg. Psychiatry 85 (2), 135–142.
Johansen-Berg, H., Gutman, D.A., Behrens, T.E.J., Matthews, P.M., Rushworth, M.F.S., Katz, E., Mayberg, H.S., 2008. Anatomical connectivity of the subgenual cingulate region targeted with deep brain stimulation for treatment-resistant depression. Cereb. Cortex 18 (6), 1374–1383.
Kanai, R., Bahrami, B., Duchaine, B., Janik, A., Banissy, M.J., Rees, G., 2012. Brain structure links loneliness to social perception. Curr. Biol. 22 (20), 1975–1979.
Keysers, C., Kaas, J.H., Gazzola, V., 2010. Somatosensation in social perception. Nat. Rev. Neurosci. 11 (6), 417–428.
Kober, H., Barrett, L.F., Joseph, J., Bliss-Moreau, E., Lindquist, K., Wager, T.D., 2008. Functional grouping and cortical–subcortical interactions in emotion: a meta-analysis of neuroimaging studies. NeuroImage 42 (2), 998–1031.
Kong, X., Wei, D., Li, W., Cun, L., Xue, S., Zhang, Q., Qiu, J., 2015. Neuroticism and extraversion mediate the association between loneliness and the dorsolateral prefrontal cortex. Exp. Brain Res. 233 (1), 157–164.
Kotz, S.A., Meyer, M., Alter, K., Besson, M., von Cramon, D.Y., Friederici, A.D., 2003. On the lateralization of emotional prosody: an event-related functional MR investigation. Brain Lang. 86 (3), 366–376.
Kurth, F., Zilles, K., Fox, P.T., Laird, A.R., Eickhoff, S.B., 2010. A link between the systems: functional differentiation and integration within the human insula revealed by meta-analysis. Brain Struct. Funct. 214 (5–6), 519–534.
Lan, C.C., Tsai, S.J., Huang, C.C., Wang, Y.H., Chen, T.R., Yeh, H.L., Yang, A.C., 2015. Functional connectivity density mapping of depressive symptoms and loneliness in non-demented elderly male. Front. Aging Neurosci., *7*.
Lemche, E., Giampietro, V.P., Surguladze, S.A., Amaro, E.J., Andrew, C.M., Williams, S.C., Simmons, A., 2006. Human attachment security is mediated by the amygdala: evidence from combined fMRI and psychophysiological measures. Hum. Brain Mapp. 27 (8), 623–635.
Liu, J., Dietz, K., DeLoyht, J.M., Pedre, X., Kelkar, D., Kaur, J., Nestler, E.J., 2012. Impaired adult myelination in the prefrontal cortex of socially isolated mice. Nat. Neurosci. 15 (12), 1621–1623.
Makinodan, M., Rosen, K.M., Ito, S., Corfas, G., 2012. A critical period for social experience–dependent oligodendrocyte maturation and myelination. Science 337 (6100), 1357–1360.
Marchand, W.R., Lee, J.N., Johnson, S., Gale, P., Thatcher, J., 2013. Differences in functional connectivity in major depression versus bipolar II depression. J. Affect. Disord. 150 (2), 527–532.
Martuzzi, R., Ramani, R., Qiu, M., Shen, X., Papademetris, X., Constable, R.T., 2011. A whole-brain voxel based measure of intrinsic connectivity contrast reveals local changes in tissue connectivity with anesthetic without a priori assumptions on thresholds or regions of interest. NeuroImage 58 (4), 1044–1050.
McWhirter, B.T., 1990. Factor analysis of the revised UCLA loneliness scale. Curr. Psychol. 9 (1), 56–68.
Meyer, S., Strittmatter, M., Fischer, C., Georg, T., Schmitz, B., 2004. Lateralization in autononic dysfunction in ischemic stroke involving the insular cortex. Neuroreport 15 (2), 357–361.
Murphy, K., Birn, R.M., Handwerker, D.A., Jones, T.B., Bandettini, P.A., 2009. The impact of global signal regression on resting state correlations: are anti-correlated networks introduced? NeuroImage 44 (3), 893–905.
Nakagawa, S., Takeuchi, H., Taki, Y., Nouchi, R., Sekiguchi, A., Kotozaki, Y., Yamamoto, Y., 2015. White matter structures associated with loneliness in young adults. Sci. Rep., 5.
Nee, D.E., Wager, T.D., Jonides, J., 2007. Interference resolution: insights from a meta-

analysis of neuroimaging tasks. Cogn. Affect. Behav. Neurosci. 7 (1), 1–17.
Nelson, S.M., Dosenbach, N.U., Cohen, A.L., Wheeler, M.E., Schlaggar, B.L., Petersen, S.E., 2010. Role of the anterior insula in task-level control and focal attention. Brain Struct. Funct. 214 (5–6), 669–680.
Oldfield, R.C., 1971. The assessment and analysis of handedness: the Edinburgh inventory. Neuropsychologia 9 (1), 97–113.
Petersen, S.E., Posner, M.I., 2012. The attention system of the human brain: 20 years after. Annu. Rev. Neurosci. 35, 73.
Power, J.D., Cohen, A.L., Nelson, S.M., Wig, G.S., Barnes, K.A., Church, J.A., Schlaggar, B.L., 2011. Functional network organization of the human brain. Neuron 72 (4), 665–678.
Qualter, P., Rotenberg, K., Barrett, L., Henzi, P., Barlow, A., Stylianou, M., Harris, R.A., 2013. Investigating hypervigilance for social threat of lonely children. J. Abnorm. Child Psychol. 41 (2), 325–338.
Radloff, L.S., 1977. The CES-D scale a self-report depression scale for research in the general population. Appl. Psychol. Meas. 1 (3), 385–401.
Ridgway, G.R., Omar, R., Ourselin, S., Hill, D.L., Warren, J.D., Fox, N.C., 2009. Issues with threshold masking in voxel-based morphometry of atrophied brains. NeuroImage 44 (1), 99–111.
Rubinov, M., Sporns, O., 2010. Complex network measures of brain connectivity: uses and interpretations. NeuroImage 52 (3), 1059–1069.
Russell, D.W., 1996. UCLA loneliness scale (Version 3): reliability, validity, and factor structure. J. Pers. Assess. 66 (1), 20–40.
Ruz, M., Tudela, P., 2011. Emotional conflict in interpersonal interactions. NeuroImage 54 (2), 1685–1691.
Sadaghiani, S., D'Esposito, M., 2014. Functional characterization of the cingulo-opercular network in the maintenance of tonic alertness. Cereb. Cortex, 72, bhu072.
Sadaghiani, S., D'Esposito, M., 2015. Functional characterization of the cingulo-opercular network in the maintenance of tonic alertness. Cereb. Cortex 25 (9), 2763–2773.
Sadaghiani, S., Scheeringa, R., Lehongre, K., Morillon, B., Giraud, A.-L., Kleinschmidt, A., 2010. Intrinsic connectivity networks, alpha oscillations, and tonic alertness: a simultaneous electroencephalography/functional magnetic resonance imaging study. J. Neurosci. 30 (30), 10243–10250.
Sadaghiani, S., Scheeringa, R., Lehongre, K., Morillon, B., Giraud, A.-L., D'Esposito, M., Kleinschmidt, A., 2012. Alpha-band phase synchrony is related to activity in the fronto-parietal adaptive control network. J. Neurosci. 32 (41), 14305–14310.
Sarason, I.G., Sarason, B.R., Shearin, E.N., 1986. Social support as an individual difference variable: Its stability, origins, and relational aspects. J. Pers. Soc. Psychol. 50 (4), 845.
Seeley, W.W., Menon, V., Schatzberg, A.F., Keller, J., Glover, G.H., Kenna, H., Greicius, M.D., 2007. Dissociable intrinsic connectivity networks for salience processing and executive control. J. Neurosci. 27 (9), 2349–2356.
Shimony, J.S., Zhang, D., Johnston, J.M., Fox, M.D., Roy, A., Leuthardt, E.C., 2009. Resting-state spontaneous fluctuations in brain activity: a new paradigm for presurgical planning using fMRI. Acad. Radiol. 16 (5), 578–583.
Sim, V.L., Guberman, A., Hogan, M.J., 2005. Acute bilateral opercular strokes causing loss of emotional facial movements. Can. J. Neurol. Sci. 32 (01), 119–121.
Simmonds, D.J., Pekar, J.J., Mostofsky, S.H., 2008. Meta-analysis of Go/No-go tasks demonstrating that fMRI activation associated with response inhibition is task-dependent. Neuropsychologia 46 (1), 224–232.
Sridharan, D., Levitin, D.J., Menon, V., 2008. A critical role for the right fronto-insular cortex in switching between central-executive and default-mode networks. Proc. Natl. Acad. Sci. 105 (34), 12569–12574.
Steiger, J.H., 1980. Tests for comparing elements of a correlation matrix. Psychol. Bull. 87 (2), 245.
Steptoe, A., Shankar, A., Demakakos, P., Wardle, J., 2013. Social isolation, loneliness, and all-cause mortality in older men and women. Proc. Natl. Acad. Sci. 110 (15), 5797–5801.
Swick, D., Ashley, V., Turken, U., 2011. Are the neural correlates of stopping and not going identical? Quantitative meta-analysis of two response inhibition tasks. NeuroImage 56 (3), 1655–1665.
Thyreau, B., Schwartz, Y., Thirion, B., Frouin, V., Loth, E., Vollstädt-Klein, S., Schumann, G., 2012. Very large fMRI study using the IMAGEN database: sensitivity–specificity and population effect modeling in relation to the underlying anatomy. NeuroImage 61 (1), 295–303.
Tian, Y., Liang, S., Yuan, Z., Chen, S., Xu, P., Yao, D., 2014. White matter structure in loneliness: preliminary findings from diffusion tensor imaging. Neuroreport 25 (11), 843–847.
Tomasi, D., Volkow, N.D., 2010. Functional connectivity density mapping. Proc. Natl. Acad. Sci. 107 (21), 9885–9890.
Van Den Heuvel, M.P., Pol, H.E.H., 2010. Exploring the brain network: a review on resting-state fMRI functional connectivity. Eur. Neuropsychopharmacol. 20 (8), 519–534.
Van Dijk, K.R., Hedden, T., Venkataraman, A., Evans, K.C., Lazar, S.W., Buckner, R.L., 2010. Intrinsic functional connectivity as a tool for human connectomics: theory, properties, and optimization. J. Neurophysiol. 103 (1), 297–321.
Van Rijn, S., Aleman, A., Van Diessen, E., Berckmoes, C., Vingerhoets, G., Kahn, R.S., 2005. What is said or how it is said makes a difference: role of the right fronto-parietal operculum in emotional prosody as revealed by repetitive TMS. Eur. J. Neurosci. 21 (11), 3195–3200.
van Roekel, E., Verhagen, M., Engels, R.C., Scholte, R.H., Cacioppo, S., Cacioppo, J.T., 2016. Trait and state levels of loneliness in early and late adolescents: examining the differential reactivity hypothesis. J. Clin. Child Adolesc. Psychol., 1–12.
Vrtička, P., Andersson, F., Grandjean, D., Sander, D., Vuilleumier, P., 2008. Individual attachment style modulates human amygdala and striatum activation during social appraisal. PLoS One 3 (8), e2868.
Wang, L., Dai, Z., Peng, H., Tan, L., Ding, Y., He, Z., Li, W., 2014. Overlapping and segregated resting-state functional connectivity in patients with major depressive disorder with and without childhood neglect. Hum. Brain Mapp. 35 (4), 1154–1166.
Wei, M., Russell, D.W., Zakalik, R.A., 2005. Adult attachment, social self-efficacy, self-disclosure, loneliness, and subsequent depression for freshman college students: a longitudinal study. J. Couns. Psychol. 52 (4), 602.
Weissenbacher, A., Kasess, C., Gerstl, F., Lanzenberger, R., Moser, E., Windischberger, C., 2009. Correlations and anticorrelations in resting-state functional connectivity MRI: a quantitative comparison of preprocessing strategies. NeuroImage 47 (4), 1408–1416.
Whitfield-Gabrieli, S., Nieto-Castanon, A., 2012. Conn: a functional connectivity toolbox for correlated and anticorrelated brain networks. Brain Connect. 2 (3), 125–141.
Wilke, M., 2012. An alternative approach towards assessing and accounting for individual motion in fMRI timeseries. NeuroImage 59 (3), 2062–2072.
Wilke, M., 2014. Isolated assessment of translation or rotation severely underestimates the effects of subject motion in FMRI data. PLoS One 9 (10), e106498.
Wilson, R.S., Krueger, K.R., Arnold, S.E., Schneider, J.A., Kelly, J.F., Barnes, L.L., Bennett, D.A., 2007. Loneliness and risk of Alzheimer disease. Arch. Gen. Psychiatry 64 (2), 234–240.
Wong, N.M.L., Liu, H.L., Lin, C., Huang, C.M., Wai, Y.Y., Lee, S.H., Lee, T.M.C., 2016. Loneliness in late-life depression: structural and functional connectivity during affective processing. Psychol. Med., 1–15.
Woo, C.-W., Krishnan, A., Wager, T.D., 2014. Cluster-extent based thresholding in fMRI analyses: pitfalls and recommendations. NeuroImage 91, 412–419.
Worsley, K.J., Friston, K.J., 1995. Analysis of fMRI time-series revisited – again. NeuroImage 2 (3), 173–181.